Improved Understanding of the Link Between Catchment-Scale Vegetation Accessible Storage and Satellite-Derived Soil Water Index

Bouaziz, Laurene; Steele-Dunne, Susan; Schellekens, Jaap; Weerts, Albrecht H.; Stam, Jasper; Sprokkereef, Eric; Winsemius, Hessel H.C.; Savenije, Hubert H.G.; Hrachowitz, Markus

DOI
10.1029/2019WR026365

Publication date
2020

Document Version
Final published version

Published in
Water Resources Research

Citation (APA)
Bouaziz, L., Steele-Dunne, S., Schellekens, J., Weerts, A. H., Stam, J., Sprokkereef, E., Winsemius, H. H. C., Savenije, H. H. G., & Hrachowitz, M. (2020). Improved Understanding of the Link Between Catchment-Scale Vegetation Accessible Storage and Satellite-Derived Soil Water Index. *Water Resources Research*, *56*(3), 1-22. Article e2019WR026365. https://doi.org/10.1029/2019WR026365

Water Resources Research

RESEARCH ARTICLE
10.1029/2019WR026365

Improved Understanding of the Link Between Catchment-Scale Vegetation Accessible Storage and Satellite-Derived Soil Water Index

Laurène J. E. Bouaziz[1,2], Susan C. Steele-Dunne[1], Jaap Schellekens[3], Albrecht H. Weerts[2,4], Jasper Stam[5], Eric Sprokkereef[5], Hessel H. C. Winsemius[1,2], Hubert H. G. Savenije[1], and Markus Hrachowitz[1]

[1]Department of Water Management, Faculty of Civil Engineering and Geosciences, Delft University of Technology, Delft, Netherlands, [2]Department Catchment and Urban Hydrology, Deltares, Delft, Netherlands, [3]VanderSat, Haarlem, the Netherlands, [4]Hydrology and Quantitative Water Management Group, Department of Environmental Sciences, Wageningen University, Wageningen, Netherlands, [5]Ministry of Infrastructure and Water Management, Lelystad, Netherlands

Abstract The spatiotemporal dynamics of water volumes stored in the unsaturated root zone are a key control on the response of terrestrial hydrological systems. Robust, catchment-scale root-zone soil moisture estimates are thus critical for reliable predictions of river flow, groundwater recharge, or evaporation. Satellites provide estimates of near-surface soil moisture that can be used to approximate the moisture content in the entire unsaturated root zone through the Soil Water Index (SWI). The characteristic time length (T, in days), as only parameter in the SWI approach, characterizes the temporal variability of soil moisture. The factors controlling T are typically assumed to be related to soil properties and climate; however, no clear link has so far been established. In this study, we hypothesize that optimal T values (T_{opt}) are linked to the interplay of precipitation and evaporation during dry periods, thus to catchment-scale vegetation accessible water storage capacities in the unsaturated root zone. We identify T_{opt} by matching modeled time series of root-zone soil moisture from a calibrated process-based hydrological model to SWI from several satellite-based near-surface soil moisture products in 16 contrasting catchments in the Meuse river basin. T_{opt} values are strongly and positively correlated with vegetation accessible water volumes that can be stored in the root zone, here estimated for each study catchment both as model calibration parameter and from a water-balance approach. Differences in T_{opt} across catchments are also explained by land cover (% agriculture), soil texture (% silt), and runoff signatures (flashiness index).

Plain Language Summary The amount of water in the soil accessible to roots of plants for growth is a key element to understand and predict short- and long-term dynamics of the hydrological cycle in a river basin. Satellites provide worldwide estimates of water amounts in the first few centimeters of the soil. If the time scale of water transport from the surface to the root zone is known, this near-surface water amount can be used to estimate the water amount in the entire root zone of vegetation. We hypothesize that this time scale depends on the maximum amount of water in the soil that is accessible to roots. We show that using river discharge, rainfall, and evaporation data, we can estimate the maximum amount of water that is available to roots and, therefore, the time scale needed to estimate water amounts in the root zone from satellite estimates of water content in the first few centimeters of the soil.

Key Points:
- Time length T to infer root zone from surface soil moisture is strongly related to root-zone water storage capacity
- Root-zone water storage capacity can be inferred from available hydrometeorological data
- Soil moisture products available globally can be enhanced to meaningfully represent root-zone soil moisture

Supporting Information:
- Supporting Information S1

Correspondence to:
L. J. E. Bouaziz,
Laurene.Bouaziz@deltares.nl

Citation:
Bouaziz, L. J. E., Steele-Dunne, S. C., Schellekens, J., Weerts, A. H., Stam, J., Sprokkereef, E., et al. (2020). Improved understanding of the link between catchment-scale vegetation accessible storage and satellite-derived Soil Water Index. *Water Resources Research*, *56*, e2019WR026365. https://doi.org/10.1029/2019WR026365

Received 17 SEP 2019
Accepted 4 MAR 2020
Accepted article online 9 MAR 2020

1. Introduction

Catchment-scale estimates of water volumes stored in the unsaturated root zone are a key element regulating the partitioning of water fluxes in terrestrial hydrological systems (Savenije & Hrachowitz, 2017). The spatiotemporal dynamics of this moisture content control how much additional water can be stored in the soil of the unsaturated root zone and how much water is thus available for plant transpiration. Capillary forces in soils have the ability to retain water against gravity to delay drainage. Conversely, excess water that cannot be held against gravity is released from soils as lateral flow and/or groundwater recharge to

eventually generate the runoff response in streams. For reliable estimates of runoff, accurate estimates of soil moisture contents in the unsaturated root zone are thus required (Blöschl & Zehe, 2005).

However, in situ soil moisture observations are typically not available at sufficient spatiotemporal scales and resolutions, except for in a handful of small experimental catchments (e.g., Bogena et al., 2010). An increasing number of studies has therefore previously explored the value of globally available remotely sensed soil moisture estimates for calibration and evaluation of or assimilation in different types of hydrological models (e.g., Beck et al., 2009; Crow et al., 2005; Gevaert et al., 2018; Leroux et al., 2016; López López et al., 2016, 2017; Nijzink et al., 2018; Parajka et al., 2009; Rakovec et al., 2016; Silvestro et al., 2015; Sutanudjaja et al., 2014; Tian, 2007; Wanders et al., 2014).

The use of remotely sensed soil moisture products has proven to be relevant for a variety of hydrological applications; however, a key issue is that the raw products often lack direct hydrological relevance. Depending on the satellite mission, the soil moisture estimates are generally limited to the upper-most few centimeters of the soil. This near-surface soil moisture is in itself uninformative to quantify water release to streams, which is regulated by the integrated moisture content over the entire unsaturated root zone. Establishing a systematic quantitative link between near-surface soil moisture and the hydrologically relevant soil moisture in the unsaturated root zone is therefore of critical importance but remains challenging (Blöschl et al., 2019; McCabe et al., 2017; Sheffield et al., 2018).

Analytical, statistical, or modeling methods have been proposed to estimate soil moisture in the unsaturated root zone by smoothing and delaying the near-surface soil moisture signal (Entekhabi et al., 1994; Mahmood & Hubbard, 2007; Manfreda et al., 2014; Ragab, 1995; Sabater et al., 2007; Wagner et al., 1999). For example, Wagner et al. (1999) propose a simplified two-layer model to convolve the near-surface soil moisture signal to a Soil Water Index (SWI) using an exponential filter. The underlying assumption implies that the water fluxes from the surface through the entire root zone is proportional to the difference in soil moisture between both. Stroud (1999) and Albergel et al. (2008) reformulate the exponential filter to a recursive filter to handle data more easily than the original formulation. Despite its simplicity and lack of explicit link to physical processes, SWI provides operationally useful estimates of aggregated soil moisture content in the soil profile (Albergel et al., 2008, 2012; Brocca et al., 2010, 2011; Ceballos et al., 2005; Ford et al., 2014).

The proposed recursive filter for the SWI calculation requires a single parameter, the characteristic time length T, expressed in unit of time (usually days), which is proportional to the ratio of the depth of the reservoir below the surface and a pseudo-diffusivity coefficient. The larger the value of T, the more smoothing and delaying of the near-surface soil moisture signal occurs in the estimation of the root-zone soil moisture. The parameter T has been interpreted to be a lumped surrogate for multiple interacting processes influencing soil moisture dynamics, such as soil depth, evaporation, runoff, soil hydraulic properties, or vegetation cover (Ceballos et al., 2005).

Optimal values of the characteristic time lengths T_{opt} are often derived by relating satellite-derived SWI to observed and/or modeled soil moisture time series integrated to different depths (Albergel et al., 2008; Beck et al., 2009; Brocca et al., 2011; Ceballos et al., 2005; de Lange et al., 2008; Ford et al., 2014; Paulik et al., 2014; Wagner et al., 1999). T_{opt} values increase with increasing depth of soil moisture measurements or deeper soil moisture profiles (up to 100 cm), implying less temporal variability of soil moisture at increasing depths (Albergel et al., 2008; Ceballos et al., 2005; Paulik et al., 2014; Wagner et al., 1999; Wang et al., 2017).

To infer SWI from near-surface soil moisture in areas where no in situ soil moisture observations are available, it is important to understand the factors controlling the characteristic time length T. Previous studies assessed either soil properties and/or climate as main controls to explain the variability of T_{opt} values.

The role of climate as a control on T_{opt} was assessed by Albergel et al. (2008) and Wang et al. (2017). Albergel et al. (2008) suggest that a weak relation with climate may exist, with lower values of T_{opt} in areas with higher evaporative demand and less frequent but more intense precipitation. Wang et al. (2017) did not find a correlation with mean annual potential evaporation. However, they found a negative correlation with mean annual precipitation, suggesting that areas with mean annual precipitation larger than 500 mm year^{-1} have smaller values of T_{opt} due to stronger hydraulic connections between the surface and deeper layers.

Ceballos et al. (2005), de Lange et al. (2008), and Wang et al. (2017) found that soil texture is an important control on T_{opt}. Sandy soils enable fast drainage and low water retention as compared to clayey soils, therefore resulting in a low temporal persistence of soil moisture in the system. This implies a stronger similarity

between the near-surface and deeper soil moisture and therefore lower T_{opt} values for sandy than for clayey soils (Ceballos et al., 2005; Wang et al., 2017). On the other hand, de Lange et al. (2008) report higher T_{opt} values for sandy than clayey soils. Albergel et al. (2008) and Paulik et al. (2014) did not find a correlation between T_{opt} and fractions of clay and sand.

These contradicting findings hinder our efforts to estimate T values that represent the integrated soil moisture content in the unsaturated root zone. As a result of the inconclusive role of soil properties and climate, T_{opt} values of 20 days are often assumed from literature to represent soil moisture in the first 100 cm of the soil (Wagner et al., 1999). However, the vegetation accessible water storage, which is a key variable in hydrological applications as it controls the partitioning between drainage and evaporation, does not necessarily correspond to soil moisture in the first 100 cm of the soil.

Despite the important hydrological role of the root-zone storage capacity, it is difficult to observe it at the catchment scale. Heterogeneity within catchments impedes our ability to integrate soil and plant root properties beyond point-scale measurements. The root-zone storage capacity is, therefore, often estimated from calibration of a hydrological model, which includes a representation of this storage capacity in the dynamic part of the unsaturated root zone. However, the derived catchment representative value of root-zone storage capacity may be subject to equifinality, even if additional data are used to constrain the calibration, making it difficult to assess its plausibility (de Boer-Euser et al., 2016).

Recent studies have demonstrated that root-zone storage capacities can be estimated from the amount of water accessible to vegetation for transpiration (de Boer-Euser et al., 2016; Gao et al., 2014; Nijzink et al., 2016; Wang-Erlandsson et al., 2016). The underlying assumption is that vegetation creates a buffer large enough to fulfill evaporative demand and overcome dry spells with a certain return period to ensure their long-term survival (Eagleson & Tellers, 1982; Milly, 1994). The interplay between water supply through precipitation and evaporative water demand, accumulated over dry periods, enables us to estimate catchment-scale vegetation accessible water storage capacities in the unsaturated root-zone (Donohue et al., 2012; Gao et al., 2014; Gentine et al., 2012; Kleidon & Heimann, 1998; Nijzink et al., 2016; Schymanski et al., 2008).

The overarching aim of our study is to establish a quantitative link between optimal T values and catchment-scale vegetation accessible water storage capacities. This allows us to make informed decisions on optimal T values to meaningfully use near-surface soil moisture data in hydrological models. We first identify T_{opt} values that maximize the correlation between time series of SWI derived from several remotely sensed products and modeled root-zone soil moisture using a process-based hydrological model. We test this in 16 contrasting catchments of the Meuse river basin to highlight the large variability of T_{opt} values and therefore the need to adequately estimate T_{opt}. We then test the relation between T_{opt} and root-zone water storage capacities derived as calibrated model parameter. This is useful to emphasis the role of T_{opt} in providing root-zone soil moisture estimates consistent with their representation in hydrological applications. Finally, we use a well-established method relying on the interplay between precipitation and evaporation to independently estimate catchment-scale vegetation accessible water storage capacities (de Boer-Euser et al., 2016; Nijzink et al., 2016; Milly, 1994) and test for the relation with T_{opt} to answer our overarching hypothesis.

2. Study Area and Data

2.1. Study Area

We test our hypothesis in 16 contrasting catchments of the Meuse basin in North-West Europe, with areas varying from 127 to 551 km^2 (see Figure 1 and Table 1). The Meuse is a rain-dominated river with large intra-annual variations in seasonal runoff, mainly caused by high summer and low winter potential evaporation. In the Belgian Ardennes (IDs 1–5 in Figure 1b), snow occurs almost every year and may last for several weeks; however, snow water equivalents are relatively low, and mean annual maxima are estimated at 15 mm. Snow is, therefore, not a major component of the discharge regime (de Wit et al., 2001). Mean annual precipitation varies between 750 and 1200 mm year^{-1} across studied catchments. Potential evaporation and runoff are 620 and 420 mm year^{-1}, respectively. Elevation ranges between 50 and 700 m, and highest and steepest areas are found in the Ardennes. Main land cover types include forest (35%), agriculture (32%), pasture (21%), and urban areas (9%; Figure 1c). The Meuse basin is underlain by limestones from the Middle and Late Jurassic in the French part and relatively impermeable metamorphic Cambrian and

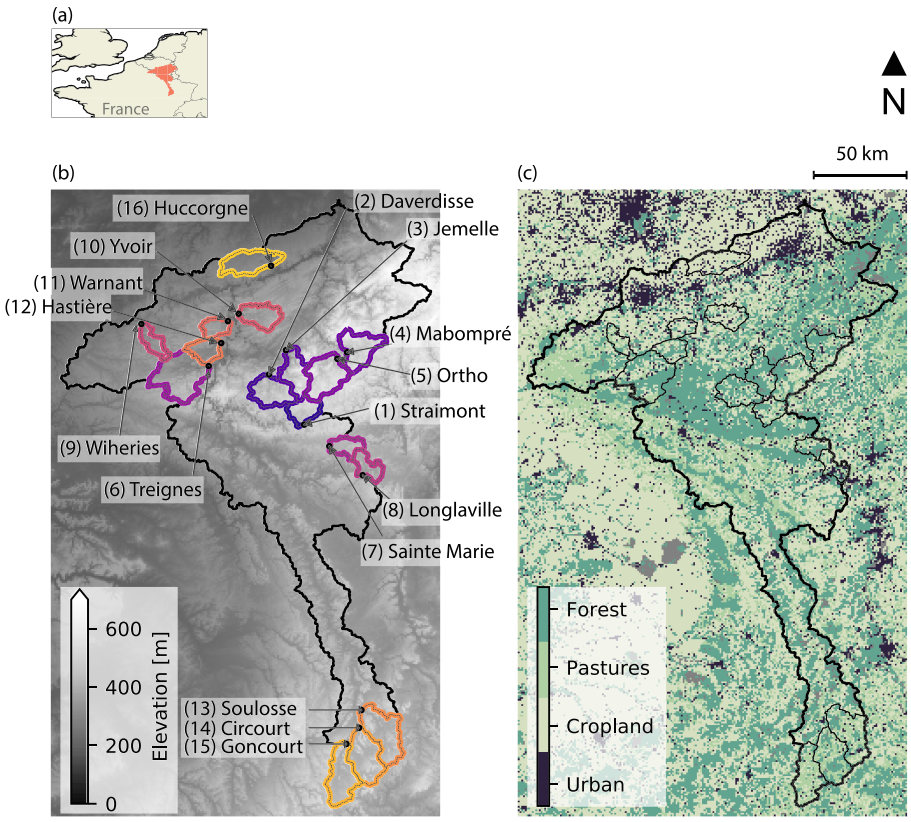

Figure 1. (a) Outline of the Meuse River Basin upstream of the city of Maastricht; (b) Digital Elevation Model and 16 studied catchments; (c) CORINE Land Cover (CLC 2012, Version 18.5.1 Büttner et al., 2014) main land cover types (coordinate reference system used is EPSG:32631, UTM31N).

Early Devonian sandstone in the Belgian Ardennes. Soil textures mainly consist of silt loam in the Ardennes and silty clay loam in France, where a higher clay fraction seems to be related to the presence of limestones (Ballabio et al., 2016).

2.2. Satellite-Based Near-Surface Soil Moisture Products

The satellite-based near-surface soil moisture products used in this study included both passive and active microwave products, for L, C, and X bands at spatial resolutions of 100 m × 100 m and 1 km × 1 km, respectively, as provided by VanderSat (https://docs.vandersat.com/index.html, https://patents.google.com/patent/WO2017216186A1/en) and Copernicus (Sentinel-1 based Surface Soil Moisture SSM1km Bauer-Marschallinger et al., 2019), as well as at spatial resolutions of 9 km × 9 km or 25 km × 25 km as provided by the National Aeronautics and Space Administration (NASA, Entekhabi et al., 2016; Owe et al., 2008), as detailed in Table 2.

Copernicus SSM1km applies a change detection method on Sentinel-1 C-SAR backscatter values to derive relative soil moisture in percentage saturation. VanderSat products are based on the Land Parameter Retrieval Model (LPRM van der Schalie et al., 2016) method to estimate near-surface soil moisture, using descending overpasses at 6 a.m. for the Soil Moisture Active Passive satellite (SMAP) and 1.30 a.m. for the Advanced Microwave Scanning Radiometer 2 (AMSR2). The NASA SMAP Level-3 SPL3SMP-E product (Entekhabi et al., 2016) is based on a composite of ascending and descending overpasses and uses the single channel algorithm to estimate soil moisture (Entekhabi et al., 2014). The NASA AMSR2 soil moisture products are based on the LPRM algorithm (Owe et al., 2008) and are available for both descending and ascending overpasses. Brocca et al. (2011) mention that some studies find higher correlations between ascending overpasses and in situ measurements, while others favor nighttime descending overpasses to take advantage of the reduced difference between surface and canopy temperature, making it relevant to assess both ascending and descending overpasses in this study.

Table 1
Mean Annual Precipitation (P), Potential Evaporation (E_P), Runoff (Q), Aridity Index (E_p/P), Runoff Ratio (Q/P), and Flashiness Index (I_f) for Hydrological Years 2006–2011 and Catchments characteristics, Including Percentage Forest (for.) and Agriculture Cover (agr.); Percentage of Highly Productive and Fissured Aquifers (fiss.) Based on the International Hydrogeological Map of Europe (IHME, https://www.bgr.bund.de/*); Percentage Clay, Sand, and Silt (Ballabio et al., 2016), Catchment Area, Drainage Density (dd), and Mean Slope, of Study Catchments With IDs Sorted on Aridity Index From the Most to the Least Humid Catchment*

(ID) Station	P	E_p	Q	E_p/P	Q/P	I_f	for.	agr.	fiss.	clay	sand	silt	area	dd	slope
	mm year^{-1}			%	%	%	%	%	%	%	%	%	km^2	km^{-1}	%
(1) Straimont	1,187	574	621	50	52	17	34	30	0	22	16	62	183	0.36	6.7
(2) Daverdisse	1,142	568	555	51	49	15	57	28	0	21	19	61	303	0.32	7.7
(3) Jemelle	1,005	563	477	56	47	18	68	20	0	20	25	55	274	0.40	9.4
(4) Mabompre	985	572	460	59	47	16	46	28	0	21	24	55	319	0.47	7.4
(5) Ortho	990	574	470	60	47	14	40	33	0	22	21	58	387	0.37	7.3
(6) Treignes	985	579	398	60	41	28	54	27	0	22	21	57	551	0.33	6.6
(7) Sainte-Marie	1,043	600	418	60	40	36	38	26	63	23	17	60	144	0.28	4.4
(8) Longlaville	971	608	440	65	45	39	20	28	18	28	20	52	154	0.16	6.9
(9) Wiheries	889	590	356	67	40	30	19	43	0	25	15	59	140	0.33	4.9
(10) Yvoir	865	577	264	68	31	13	16	60	71	24	13	63	226	0.33	6.4
(11) Warnant	819	586	275	72	34	12	20	64	56	24	15	61	127	0.29	6.2
(12) Hastiere	802	582	285	73	36	32	41	40	0	24	21	55	169	0.40	5.4
(13) Soulosse	831	642	331	79	39	35	30	26	38	34	15	51	441	0.30	6.3
(14) Circourt	823	642	312	80	38	42	41	12	23	33	18	49	403	0.30	7.3
(15) Goncourt	815	646	295	81	36	40	19	23	19	34	14	52	376	0.27	5.6
(16) Huccorgne	737	593	181	82	25	19	3	80	16	21	9	70	307	0.25	2.6

The data of all used products were spatially averaged in the 16 catchments of the Meuse basin for the study period May 2016 until December 2017. Radio frequency interferences affect soil moisture estimations of NASA AMSR2 C1 and C2 bands and Copernicus Sentinel-1 C-band Synthetic Aperture Radar (SAR) products for January 2015 until May 2016, and this period was, therefore, left out from the analyses. Whenever mean daily catchment temperature (see section 2.4) dropped below 1 °C, near-surface soil moisture estimates were set to missing to avoid potential biases resulting from frozen soils.

2.3. Soil Water Index

The SWI approach estimates time series of soil moisture in deeper layers from antecedent satellite-based near-surface soil moisture estimates. The approach relies on a two-layer water balance model, where the

Table 2
Satellite Surface Soil Moisture Products With Associated IDs (Where d Indicates Downscaled High-Resolution Product), Provider, Sensor, Band (Where C1 and C2 Corresponds to 6.9 and 7.3 GHz, Respectively), Method or Product Name, Overpass, Resolution, and Range of Observation Count per Catchment Between May 2016 and December 2017 (Nr. obs.)

ID	Provider	Sensor	Band	Method/ Product	Overpass	Resol. km^2	Nr. obs.
S1-CSAR	Copernicus	Sentinel-1	C-SAR	SSM1km	6 a.m. 6 p.m.	1 × 1	199–290
SMAP-L-am_d	VanderSat	SMAP	L	LPRM	6 a.m.	0.1 × 0.1	297–415
SMAP-L	NASA	SMAP	L	SPL3SMP-E	6 a.m. 6 p.m.	9 × 9	316–345
AMSR2-X-am_d	VanderSat	AMSR2	X	LPRM	1.30 a.m.	0.1 × 0.1	511–572
AMSR2-X-am	NASA	AMSR2	X	LPRM	1.30 a.m.	25 × 25	508–556
AMSR2-X-pm	NASA	AMSR2	X	LPRM	1.30 p.m.	25 × 25	495–570
AMSR2-C1-am_d	VanderSat	AMSR2	C1	LPRM	1.30 a.m.	0.1 × 0.1	511–571
AMSR2-C1-am	NASA	AMSR2	C1	LPRM	1.30 a.m.	25 × 25	508–556
AMSR2-C1-pm	NASA	AMSR2	C1	LPRM	1.30 p.m.	25 × 25	495–570
AMSR2-C2-am	NASA	AMSR2	C2	LPRM	1.30 a.m.	25 × 25	508–556
AMSR2-C2-pm	NASA	AMSR2	C2	LPRM	1.30 p.m.	25 × 25	495–570

upper layer represents the near-surface soil moisture and the bottom layer is a deeper reservoir with length L only in contact with the surface layer. The soil moisture content in the deeper layer is fed by infiltration from the upper layer and is therefore explained by past dynamics, where more recent events have a stronger influence. This model assumes that the water flux from the surface through the entire deeper layer is proportional to the difference in soil moisture between the two layers, as shown by equation (1):

$$L \cdot \frac{\mathrm{d}W(t)}{\mathrm{d}t} = C \cdot (W_s(t) - W(t)), \tag{1}$$

with W the moisture content in the lower reservoir ($m^3\ m^{-3}$ or percentage saturation), L the depth of the reservoir [m], W_s the surface soil moisture content ($m^3\ m^{-3}$ or percentage saturation), and C represents a pseudo-diffusivity coefficient dependent on soil moisture and is assumed constant [m day^{-1}]. The equation is solved by assuming a constant parameter T [d], which increases with increasing soil depth or decreasing pseudo-diffusivity constant (equation (2)).

$$T = \frac{L}{C} \tag{2}$$

As only parameter in the SWI, the T value is referred to as the characteristic time length. More smoothing and delaying of the near-surface soil moisture signal occurs as the T value increases.

Stroud (1999) and Albergel et al. (2008) solve the differential equation in a recursive form (equation 3) to handle the irregular time steps of satellite near-surface soil moisture data more easily than the original exponential filter proposed by Wagner et al. (1999). Details are provided in section S1 in the supporting information.

$$SWI(t_n) = SWI(t_{n-1}) + K_n \cdot (SSM(t_n) - SWI(t_{n-1})), \tag{3}$$

where SWI, the Soil Water Index at time t_n, has replaced the continuous W and SSM, the near-surface soil moisture estimate at time t_i, has replaced the continuous W_s (all in $m^3\ m^{-3}$ or percentage saturation).

The gain K_n [−] at time t_n is given by the following recursive formula:

$$K_n = \frac{K_{n-1}}{K_{n-1} + e^{-\frac{(t_n - t_{n-1})}{T}}}, \tag{4}$$

with initial values $SWI(t_0) = SSM(t_0)$ and $K_0 = 1$ and where t_n and t_{n-1} are the observation times of the current and previous SSM observation in Julian days. The gain K_n ranges between [0, 1]. When many observations during the characteristic time length T are available, the gain will be small, meaning that the prior value will only be changed slightly toward the new observation. On the other hand, when no data have been received in quite some time relative to T, the gain will be large, implying that the new estimate of SWI will converge toward the value of the new observation. Therefore, the T value dictates how strongly previous near-surface soil moisture observations influence the current SWI.

For each of the products and study catchments, we calculate time series of daily catchment average SWI from near-surface soil moisture for values of T varying between 1 and 100 days (with time step of 1 day), according to the recursive formulation (equation (3)) for the period May 2016 to December 2017. Spin-up effects are reduced by starting the SWI calculation at the start of 2016.

2.4. Meteorological and Runoff Data

Hourly precipitation data from stations of Meteo France and the Service Public de Wallonie ((Service Public de Wallonie, 2018), https://voies-hydrauliques.wallonie.be/opencms/opencms/fr/hydro/Archive/annuaires/index.html) are spatially interpolated using climatological monthly background grids (van Osnabrugge et al., 2017) and then spatially averaged over the catchments for a calibration (2006–2011) and evaluation (2012–2017) period. Potential evaporation is estimated based on the Makkink equation (Hooghart & Lablans, 1988) and relies on hourly interpolated temperature station data (provided by the Service Public de Wallonie and retrieved from the archive of the Dutch operational flood forecasting system) and radiation grids from the Satellite Application Facility on Land Surface Analysis (LSA SAF Trigo et al., 2011). Daily observed river discharge for stations in France (IDs 8 and 13–15) are retrieved from Hydro Banque (Banque Hydro, 2018, https://hydro.eaufrance.fr/) and are provided by the Service Public de Wallonie for Belgium (IDs 1–7, 9–12, and 16).

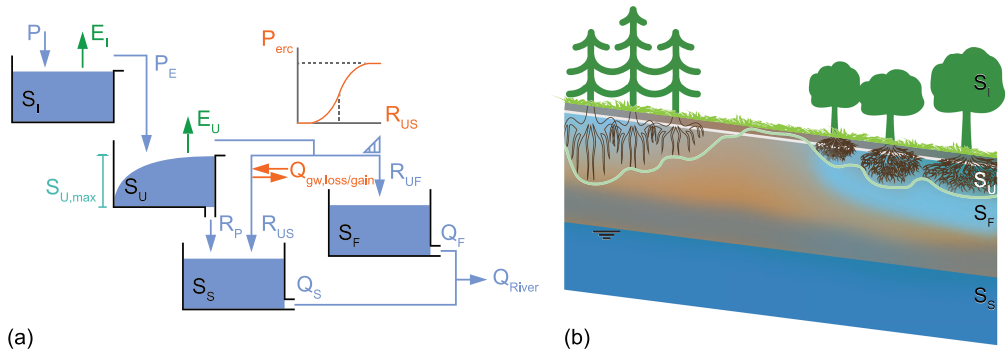

Figure 2. (a) Hydrological model with root-zone soil moisture S_U (mm, variable in time) and root-zone water storage capacity $S_{U,max}$ (mm, calibrated and constant in time) (b) associated perceptual model, where the area above the green curve represents the root-zone storage capacity. Both S_U and $S_{U,max}$ are spatially heterogeneous but aggregated to lumped effective values for each individual catchment. We define P as precipitation, P_E as effective precipitation, E as evaporation, R as an internal flux, Q as surface or subsurface drainage (all in mm day^{-1}), and S as storage (in mm). For the subscripts, we define $_I$ as interception, $_U$ as unsaturated root zone, $_S$ as slow response, $_F$ as fast response, $_P$ as percolation, and $_{gw,loss/gain}$ as net groundwater losses or gains. The parameter p_{erc} defines the maximum percentage of recharge as net groundwater losses or gains.

Runoff data between March and mid-June 2013 were discarded from the analysis due to implausibly high runoff compared to observed precipitation amounts at all stations except in the Vair at Soulosse-sous-Saint-Élophe (ID 13), Mouzon at Circourt-sur-Mouzon (ID 14) and Meuse at Goncourt (ID 15) (Bouaziz et al., 2018).

3. Methods

Section 3.1 describes the setup of a process-based lumped hydrological model to compute soil moisture time series. Section 3.2 details the methodology to derive water-balance estimates of root-zone storage capacities. Subsequently in section 3.3, the optimal characteristic time lengths (T_{opt}) in the 16 study catchments are derived using the retained set of feasible model-generated time series of daily soil moisture contents in the unsaturated root zones (S_U). In section 3.4, we then test for a relation between root-zone water storage capacity ($S_{U,max}$) inferred from the set of calibrated model parameters $S_{U,max}$ retained as feasible for each study catchment and from a water-balance approach. We also assess how the interactions between soil texture, land cover, hydrometeorological variables, runoff signatures, geological features, and topographical indices explain the variability in T_{opt} between catchments.

3.1. Hydrological Model

A process-based lumped hydrological model (Figure 2a) is set up and calibrated for each of the 16 study catchments to estimate the dynamics of catchment-scale, daily soil moisture content in the unsaturated root zone. The model consists of four storage components, namely, an interception reservoir (S_I), a reservoir representing the unsaturated root zone (S_U), a fast-responding reservoir (S_F), and a slow-responding reservoir representing the groundwater (S_S); Figure 2b. The storage components are linked through water fluxes, which also include losses to or gains from deep groundwater, which can be a significant factor in the water balance in the headwaters of the Meuse basin (Bouaziz et al., 2018). This model was selected because of the satisfying performance achieved in catchments of the Meuse (Bouaziz et al., 2018). The model has 12 calibration parameters and resembles in its core formulation FLEX-type model concepts, in the past successfully used in a wide range of environments (Euser et al., 2015; Fenicia et al., 2006, 2008; Fovet et al., 2015; Hrachowitz et al., 2014; Mostbauer et al., 2018; Nijzink et al., 2016; Nijzink et al., 2016).

The model was run at hourly time steps, which were aggregated to daily for model calibration, postcalibration evaluation, and further analyses. After a 1-year warm-up period in 2006, the model was calibrated for the January 2007 to December 2011 period, based on a multiobjective calibration strategy (Hulsman et al., 2019). The parameter space was explored with a Monte Carlo approach, sampling 10^5 realizations from uniform prior parameter distributions. Similar to Bouaziz et al. (2018), feasible parameter sets were retained based on their ability to simultaneously and adequately reproduce six different aspects of the observed hydrograph including daily flows (Q), the logarithm of the daily flows (log(Q)), the logarithm of the flow duration

curves (FDC, log(Q)), and the time series of weekly (RC,w), monthly (RC,m), and seasonal (RC,s) runoff ratios. This calibration approach was followed to limit uncertainties in medium- to long-term partitioning between drainage and evaporative fluxes and to thus approximate at least longer-term conservation of energy (Hrachowitz & Clark, 2017). All the six above described modeled variables were evaluated against their observed values based on their associated Nash-Sutcliffe Efficiencies (E_{NS}) as objective functions. Feasible parameter sets were retained when E_{NS} scores of all six variables were at least above the 90th percentile best value. For evaluation, the model was tested without further calibration in an independent period from January 2012 to December 2017 based on the same performance metrics as above. All relevant model equations as well as prior and posterior parameter ranges are provided in sections S2 and S3. For each catchment, results from an additional run optimized with the Shuffled Complex Evolution method developed at the University of Arizona (Duan et al., 1994) were within the range of the ensemble of selected parameter sets, as shown in section S4.

3.2. Derivation of the Water-Balance-Derived Root-Zone Storage Capacity

While hydrological models estimate root-zone storage capacities through an inverse process of calibration with associated risk of equifinality, the water balance approach directly infers root-zone storage capacities from hydrometeorological data. The absence of calibration considerably limits computational power and calculation time of the water-balance approach. Daily time series of precipitation and potential evaporation are used as inputs in combination with an estimate of long-term runoff ratio, while a thorough calibration of a hydrological model would also require daily time series of runoff to constrain the model parameters.

More importantly, there is increasing evidence that catchment-scale root-zone water storage capacities $S_{U,max}$ can be robustly and readily estimated following this water-balance approach (de Boer-Euser et al., 2016; Gao et al., 2014; Nijzink et al., 2016; Wang-Erlandsson et al., 2016). This root-zone storage capacity reflects the integrated interactions between atmospheric water supply and vegetation water demand as controlled by energy supply (i.e., potential evaporation) and vegetation type within a specific spatial domain (here: catchment). It should be clear that the root-zone storage capacity is not necessarily related to root depth but rather to root density as it reflects the pore volume within the influence area of roots (de Boer-Euser et al., 2016; Gentine et al., 2012; Schenk & Jackson, 2002). The underlying assumption implies that vegetation adapts its storage to overcome dry spells with certain return periods (Donohue et al., 2012; Gentine et al., 2012; Kleidon & Heimann, 1998; Milly, 1994).

The approach requires to estimate daily actual transpiration, as it depletes the root-zone storage during dry periods. We first derive the long-term actual transpiration from the water balance of the catchment:

$$\bar{E}_U \approx \bar{P} - \bar{E}_I - \bar{Q}_{River} - \bar{Q}_{gw,loss} \quad (5)$$

with long-term annual mean actual transpiration $\bar{E}_U$, precipitation $\bar{P}$, interception evaporation $\bar{E}_I$, runoff Q_{River}, and potential deep groundwater losses $\bar{Q}_{gw,loss}$, all provided in mm year^{-1}.

An interception reservoir is simulated to quantify effective precipitation $\bar{P}_E$ that reaches the soil, interception evaporation, and storage, as a function of the interception storage capacity (I_{max}; see section S2 for the detailed equations). Due to the lack of more detailed information, we quantified the effect of different interception storage capacities in a sensitivity analysis, that is, I_{max} = 0.5, 1.0, 2.0, and 3.0 mm.

If the difference between mean annual precipitation and runoff exceeds potential evaporation, catchments are likely affected by deep groundwater losses, as they were shown to be significant in several catchments of the Meuse (Bouaziz et al., 2018). We estimate mean annual deep groundwater losses with the Budyko/Turc-Mezentsev framework (Budyko, 1961; Mezentsev, 1955; Turc, 1954). Long-term mean annual actual transpiration can then be determined from mean annual effective precipitation, runoff, and where applicable groundwater losses (equation (5)).

Daily actual transpiration is subsequently scaled to the daily signal of potential evaporation after removal of the interception evaporation. This scaling allows us to introduce seasonality in actual transpiration.

The storage deficits are then calculated by accumulating the difference between effective precipitation and transpiration assuming an "infinite reservoir". The initial deficit is assumed to be zero at the start of the calculation, that is, end of the wet period. The deficit increases when transpiration exceeds effective precipitation during summer until it becomes zero again when all excess water is assumed to drain away as direct runoff. The annual maximum cumulative deficit ($S_{U,clim}$) between the time where the deficit equals zero

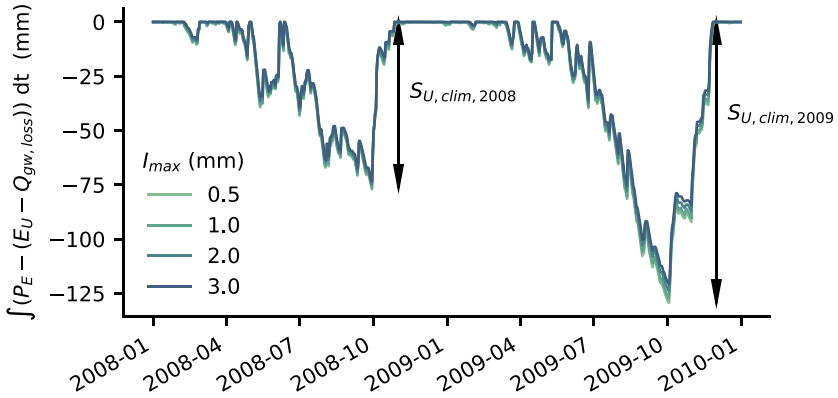

Figure 3. Annual maximum cumulative storage deficits $S_{U,clim}$ calculated from estimated daily effective precipitation, transpiration, and groundwater losses for two consecutive years and several values of the interception capacity (I_{max}) in the Hermeton catchment at Hastière (ID 12).

until the time where the total deficit returns to zero is illustrated in Figure 3 for two consecutive years. The maximum storage deficit decreases as the maximum interception capacity increases because more water is intercepted and less goes to transpiration. However, the magnitude of the fluctuations due to interception is minor relative to the magnitude of the storage deficits, as shown in Figure 3.

The annual maxima of the storage deficit $S_{U,clim}$ are fitted to the extreme value distribution of Gumbel. Following Gao et al. (2014) and Nijzink et al. (2016), the 20-year drought return period is used to estimate the water-balance-derived root-zone moisture capacity $S_{U,max}$ for each catchment using hydrometeorological data between 2006 and 2011. The detailed equations for the calculation are provided in section S5.

3.3. Identifying the Optimal Characteristic Time Length (T_{opt})

Spearman rank correlations are calculated between time series of daily SWI for T values ranging from 1 to 100 days and modeled time series of daily soil moisture content in the unsaturated root zone S_U (from section 3.1; Figures 2a and 2b). This calculation is done for each catchment, each parameter set kept as feasible and each satellite soil moisture product for the period May 2016 to December 2017, when all products are available. The optimal T value maximizes the median Spearman rank correlation between SWI and S_U across the feasible model realizations and provides the best representation of the moisture content in the unsaturated root zone. We use a variety of remotely sensed products to understand how much of the variability in T_{opt} is related to the product itself. For comparison, the Spearman rank correlation between raw and thus unfiltered values of the near-surface soil moisture SSM (note: $\lim_{T \to 0} SWI(t) = SSM(t)$) and the modeled root-zone soil moisture content S_U is also calculated for each product and catchment. Also note that the strong seasonal cycle of both variables, SWI and S_U, may excessively inflate Spearman rank correlation coefficients; however, with less than 2 years of data, it remains problematic to meaningfully discount seasonality from the time series.

3.4. Understanding Controls of the Optimal Characteristic Time Length (T_{opt})

We first test the relation between T_{opt} and root-zone storage capacities derived as calibrated parameters for the studied catchments by calculating Spearman rank coefficients for each remotely sensed product. Catchments with relatively small water storage capacities are expected to show a high variability of integrated soil moisture from one time step to another, while catchments with relatively large storage capacities are likely to show a more damped response. Indeed, a small water storage capacity is likely to fill through precipitation and empty through evaporation and drainage more rapidly than a large water storage capacity, leading to an increased variability in time. This is also in line with equation (2), where T is proportional to the depth of the reservoir below the surface.

We then test the relation between T_{opt} and root-zone storage capacities derived from the water-balance approach using meteorological and runoff data for each catchment. We also compare calibrated and water-balance derived root-zone water storage capacities between each other.

Finally, we go beyond our main hypothesis and also test the link between T_{opt} and hydrometeorological variables, land cover, soil texture, geological features, topographic indices, and runoff characteristics

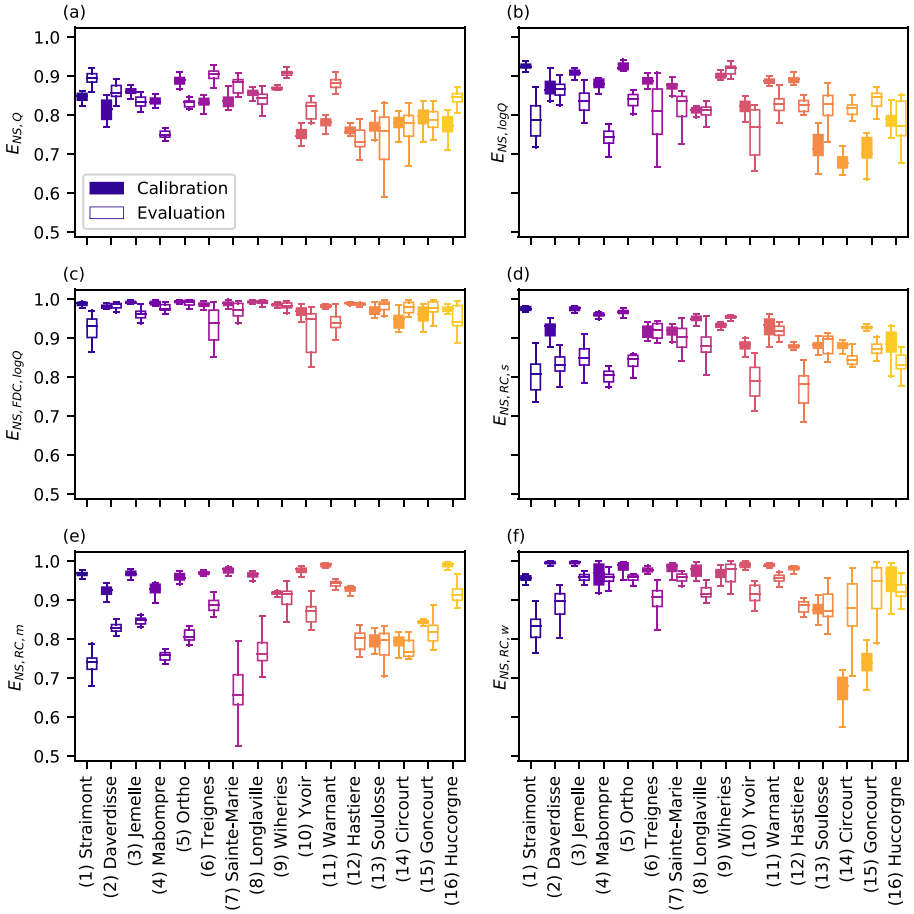

Figure 4. Calibration (filled boxplot) and evaluation (no fill) performances of Nash-Sutcliffe efficiencies of the (a) flows; (b) logarithm of the flows; (c) flow duration curve of the logarithm of the flows; (d) seasonal runoff ratio; (e) monthly runoff ratio; and (f) weekly runoff ratio for the 16 study catchments (colors as in Figure 1b).

(provided in Table 1) to further explain the observed differences in T_{opt} values between catchments. Similarly to Wang et al. (2017), we consider mean annual precipitation and potential evaporation. Additionally, we assess the link with runoff ratio, aridity index, and percentage of forest and agriculture. We also assess the relation between T_{opt} and soil texture (clay, sand, and silt percentages), as it has been the subject of several studies (Albergel et al., 2008; de Lange et al., 2008; Wang et al., 2017) and to the presence of highly productive aquifers including karstified rocks (based on the International Hydrogeological Map of Europe, IHME, https://www.brg.bund.de/). As topography is related to climate, land cover, and soil characteristics, especially in natural landscapes (Savenije & Hrachowitz, 2017), we include catchment size, drainage density, and mean slope as potential predictors to explain the variability in T_{opt} between catchments. While T_{opt} characterizes the temporal variability of soil moisture, the flashiness index (I_f) is a measure of the responsiveness of a catchment in terms of the variability of its streamflow from one time step to another (Fenicia et al., 2016). We therefore test for a relation between the flashiness index and T_{opt}, as slow dynamics in root-zone soil moisture can be expected to result in a smooth runoff response.

4. Results

4.1. Model Evaluation

The calibration and evaluation performance, in terms of the six objective functions, have rather similar performances in both periods except for some modest divergence of the models ability to reproduce runoff ratios for the evaluation period in several catchments (Figure 4). $E_{NS,Q}$ during evaluation ranges between

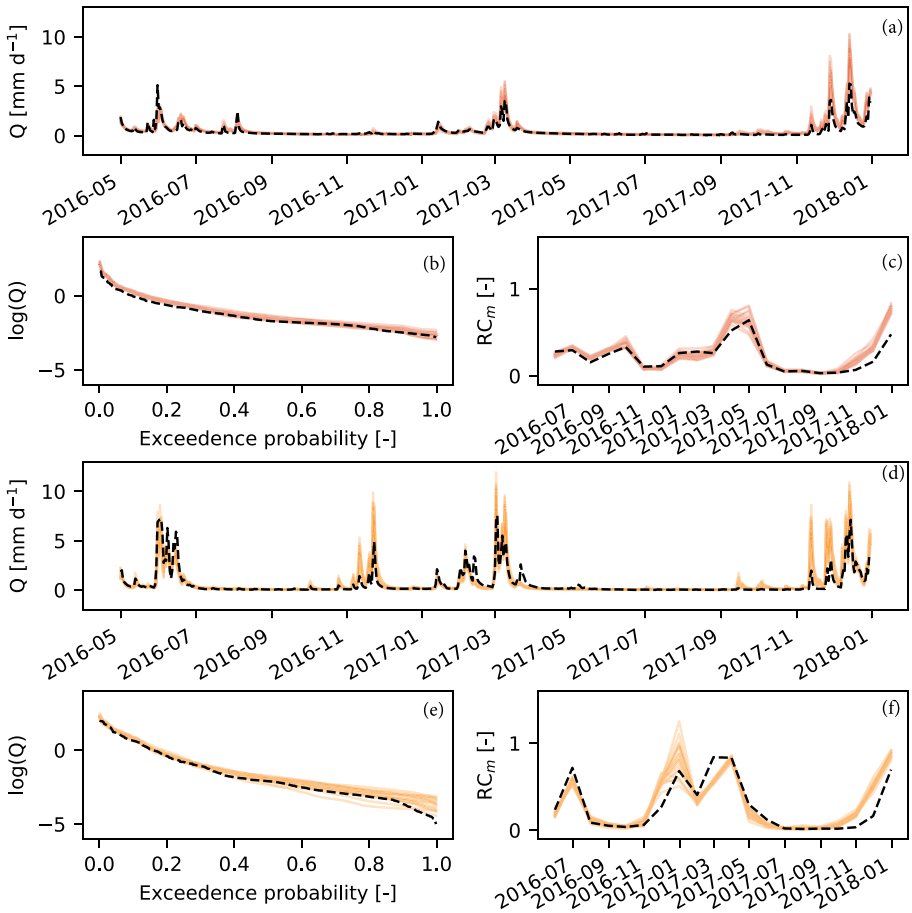

Figure 5. Observed (dashed black lines) and feasible modeled (colored lines) hydrographs for the period with available SSM data (May 2016 to December 2017), and associated flow duration curves of the log of the flows and monthly runoff ratios for (a–c) the Hermeton at Hastière (ID 12) and (d–f) the Mouzon at Circourt-sur-Mouzon (ID 14) (colors as in Figure 1b).

0.51 and 0.93 for all catchments with a mean of 0.83, while $E_{\mathrm{NS,RC,m}}$ ranges between 0.52 and 0.97 with a mean of 0.82. The model slightly overestimates peak flows (Figures 5a and 5d) but reproduces flow duration curves (Figures 5b and 5e) and monthly runoff ratios (Figures 5c and 5f) relatively well (see section S6 for all other catchments).

Overall, the models can reproduce high and low flow metrics quite well and exhibit plausible long-term partitioning of water fluxes into runoff and actual evaporation (i.e., $E_A = E_I + E_U$), according to runoff ratio, enabling us to use soil moisture S_{U} and $S_{\mathrm{U,max}}$ for the subsequent analyses.

4.2. Variability of Identified T_{opt}

Highest Spearman rank correlation coefficients r between time series of daily SWI and time series of modeled root-zone soil moisture S_{U} are obtained for T values between 6 and 32 days (median of 18 days) per soil moisture product for one illustrative catchment (see Figure 6). Figures for all other study catchments are provided in section S7. The maximum Spearman rank correlation achieved with the SWI is always higher than with the near-surface soil moisture SSM (Figure 6), as also found by Paulik et al. (2014). Especially for S1-CSAR, the Spearman rank correlation from SSM to SWI increases on average (over all catchments) from 0.54 to 0.83, as opposed to an increase from 0.75 to 0.88 for SMAP-L-am_d, possibly related to higher variance of the SSM signal of S1-CSAR compared to SMAP-L-am_d (see section S8). Introducing noise to near-surface soil moisture time series indeed leads to a larger increase in Spearman rank correlations from SSM to SWI and slightly higher T_{opt} values, suggesting noise filtering by the SWI (see section S9). The narrow band in Figure 6 suggests that Spearman rank correlations are not very sensitive to the uncertainty in model parameters, implying relatively similar root-zone soil moisture dynamics between parameter sets.

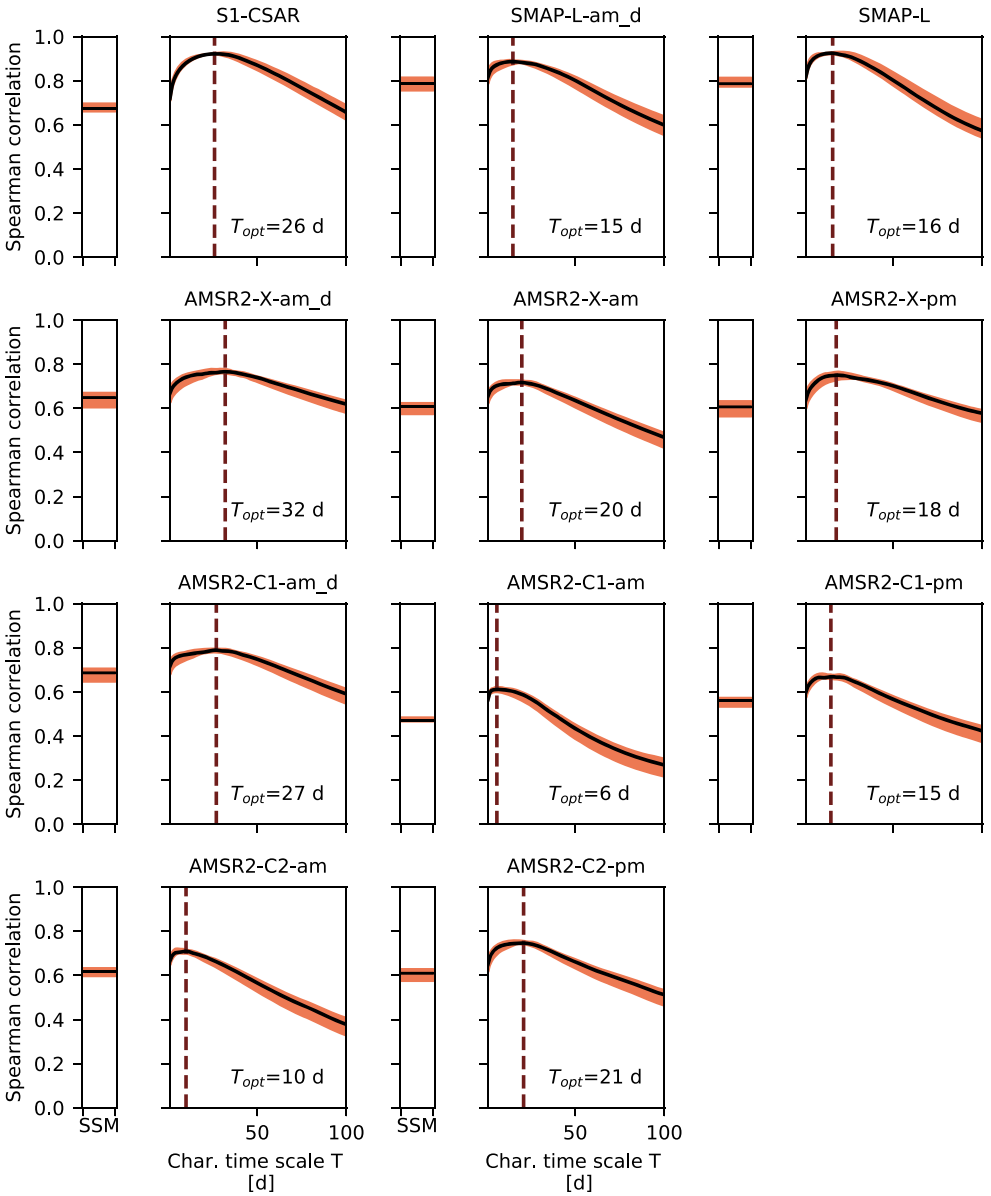

Figure 6. Spearman rank correlations coefficients between time series of modeled daily root-zone soil moisture S_U [mm] and SWI [−] for different values of the characteristic time scale T [d] in the Hermeton at Hastière (ID 12) for the period May 2016 to December 2017 for each soil moisture product. In the narrow subplots on the left side of each larger subplot, the correlation of the time series of daily near-surface soil moisture SSM and modeled root-zone soil moisture S_U is shown. The black line and colored band represent the median value and associated 25th to 75th percentiles of S_U from the ensemble of parameter sets retained as feasible. The vertical dashed line indicates the optimal value of the characteristic time scale T_{opt} [d] here defined to be at the highest correlation of the median value.

Figure 7 shows modeled daily root-zone moisture S_U for each parameter set kept as feasible, near-surface soil moisture SSM and SWI as inferred from a selection of satellite products using the associated T_{opt} (see Figure 6) for two of the 16 study catchments. All other catchments are shown in section S10. Higher values of T_{opt} lead to more smoothing and delaying of the original near-surface soil moisture signal (Figures 7b–7e vs. 7g–7j showing the effect of T_{opt} of 6–26 days vs. 2–6 days) and can therefore reproduce daily fluctuations of the modeled soil moisture S_U reasonably well (Spearman rank correlations $r > 0.82$ for the best performing products S1-CSAR and SMAP L-band products vs. $r > 0.61$ for the poorer performing AMSR2-C1-am product). For the S1-CSAR product in the Hermeton catchment at Hastière (ID 12), the variance decreases

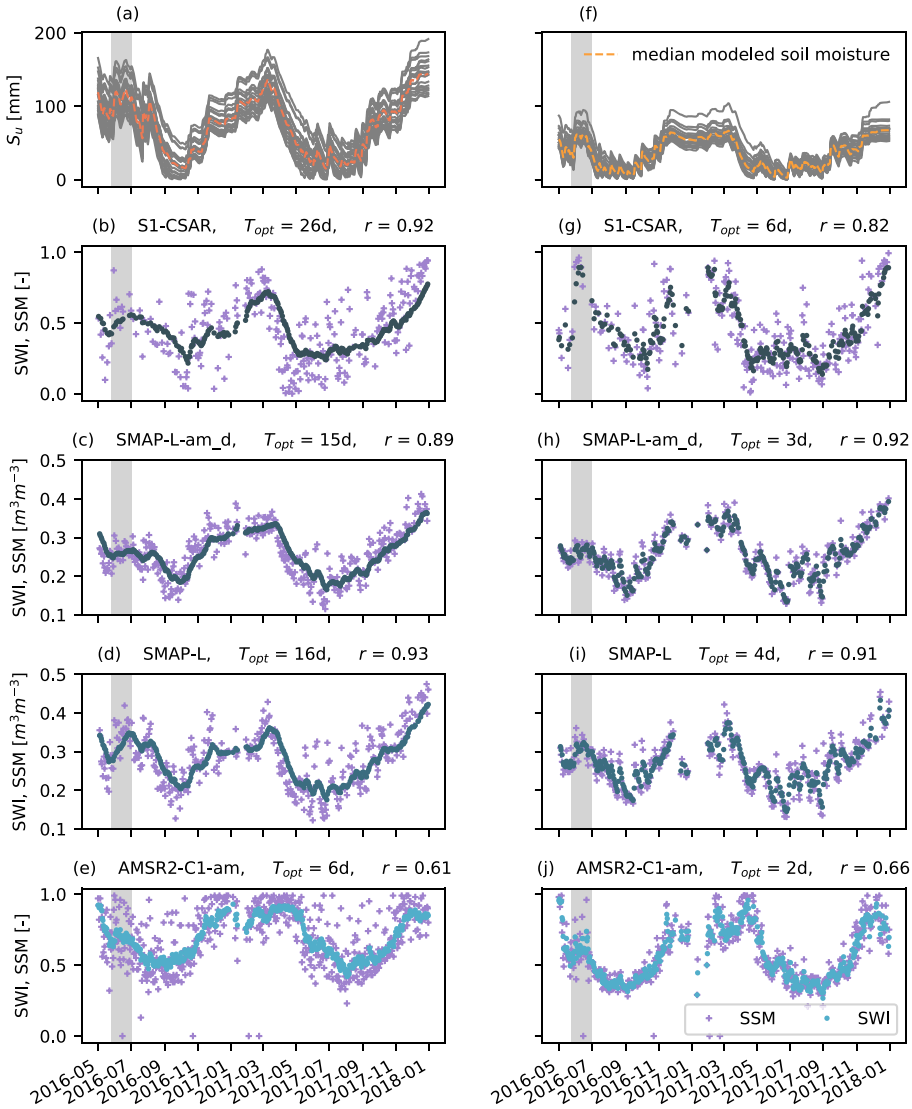

Figure 7. Time series of (a and f) modeled root-zone soil moisture S_U for all model parameter sets retained as feasible; (b–e and g–j) SSM and SWI based on the respective T_{opt} values for a selection of products with highest performance (S1-CSAR, SMAP-L-am_d, and SMAP-L) and lowest performance (AMSR2-C1-am) for (a-e) the Hermeton catchment at Hastière (ID 12); and (f–j) the Mouzon catchment at Circourt-sur-Mouzon (ID 14). The gray shaded area in summer 2016 indicates a series of very wet events. Units vary between soil moisture products as they are either provided as volumetric weights [m^3 m^{-3}] or percentage saturation [–]. The blue shades used for each soil moisture product follow the color scheme of Figures 8a and 8c.

from 0.066 for near-surface soil moisture SSM to 0.034 for SWI, while a reduction of variance from 0.065 to 0.046 can be seen for the Mouzon at Circourt-sur-Mouzon (ID 14).

During the wetting phase in the catchment of the Hermeton at Hastière (ID 12), S1-CSAR (Figure 7b) and SMAP-L (Figure 7d) have the highest visual similarity with modeled root-zone moisture S_U (Figure 7a), while the drying phase behavior is best reproduced by SMAP-L-am_d (Figure 7c) and SMAP-L (Figure 7d). Noise in AMSR2-C1-am occurs in the Hermeton at Hastière (ID 12), possibly caused by radio frequency interference (RFI) in the area. More spread in SSM of S1-CSAR is also observed compared to SSM of the L-band products (Figures 7b and 7g vs. Figures 7c–7d and 7h–7i, and section S8).

Note that in the month following 22 May 2016, a series of heavy and long-lasting precipitation events occurred over France and Belgium, with total monthly volumes between 146 and 236 mm month^{-1} over the study catchments. Despite the large spatial scale of these events, most satellite products only show a limited

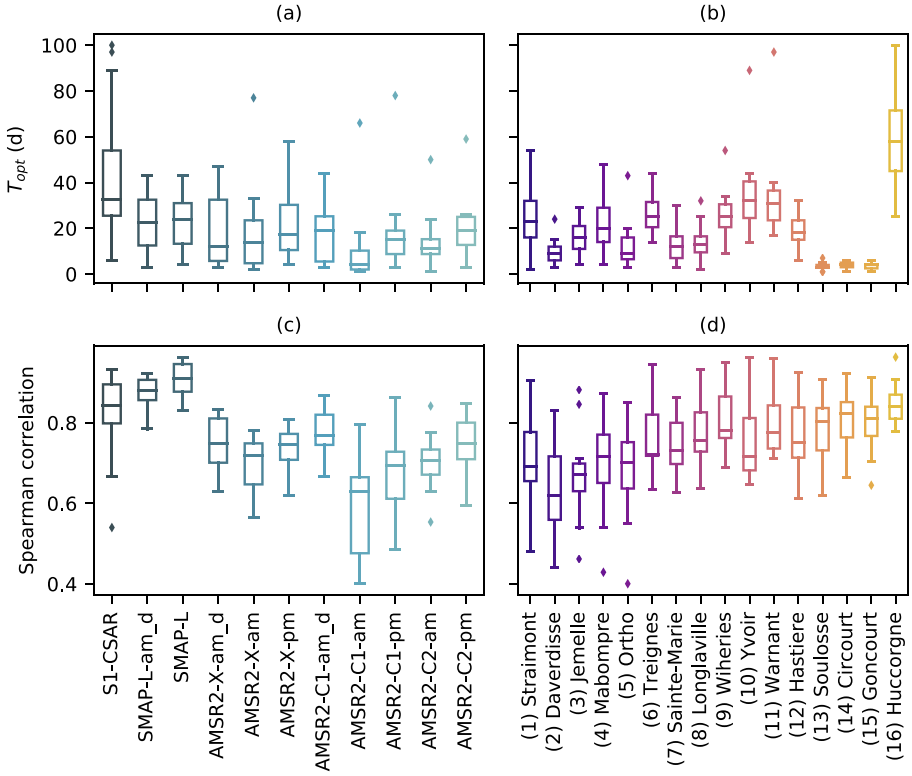

Figure 8. (a) T_{opt} range across the 16 study catchments per product. (b) T_{opt} range across all products per catchment. (c) Spearman rank correlations coefficients between SWI using the optimal T value and modeled time series of root-zone soil moisture S_U for the period May 2016 to December 2017 per product for all 16 catchments. (d) Spearman rank correlations coefficients between SWI using the optimal T value and time series of modeled root-zone soil moisture S_U for the period May 2016 to December 2017 per catchment for all products.

increase in soil moisture, except S1-CSAR, in particular in the Mouzon at Circourt-sur-Mouzon (Figure 7g). The underlying reason remains unclear.

T_{opt} varies per product (Figures 6 and 8a) with lowest 5th and highest 95th percentiles of 1 and 98 days (median of 17.5 days), with product AMSR2-C1-am showing the lowest T_{opt} (5th/95th percentiles of 1 and 30 days with a median of 4 days) and product S1-CSAR the highest values (5th/95th percentiles of 6 and 98 days with a median of 33 days). The higher T_{opt} of the only radar (active microwave) S1-CSAR product among radiometers (passive microwave) are likely related to the different sensing techniques, the larger initial variance of the SSM data compared to variances of the passive products (see sections S8 and S9) and to the larger sampling intervals (see Table 2). de Lange et al. (2008) investigated the influence of satellite sampling intervals on the T parameter and suggested that for larger sampling intervals, soil dynamics are less well reflected; therefore, higher values of the characteristic time scale are expected.

Similarly, T_{opt} varies across the study catchments (Figure 8b), with lowest 5th and highest 95th percentiles of 1 and 89 days (median of 17 days). The catchment of the Mehaigne at Huccorgne (ID 16) exhibits the largest values (5th/95th percentiles of 33.5 and 89 days with a median of 58 days); this catchment is characterized by 80% agriculture cover, relatively low runoff coefficient (25%) and low flashiness index (19%); see Table 1. The Bocq at Yvoir (ID 10) and the Molignée at Warnant (ID 11), catchments with relatively similar characteristics, also show high outlier values of T_{opt} (Figure 8b). The three most upstream catchments (IDs 13–15) exhibit the lowest T_{opt} values (5th/95th percentiles of 1 and 6 days with a median of approximately 3 days), and these catchments are, on the other hand, more responsive in time (relatively high flashiness indices varying between 35% and 42%) and have relatively low agriculture cover (12–26%; Table 1).

In general, the strongest correlations with median Spearman rank correlation coefficients r between the daily times series of SWI and S_U of 0.84, 0.88, and 0.91, respectively, can be found for the S1-CSAR and

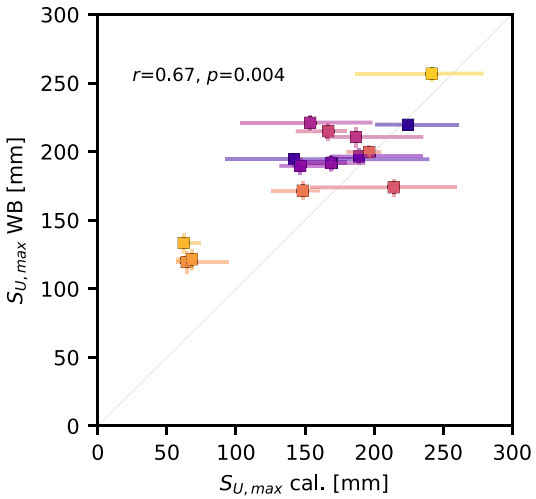

Figure 9. Relation between water-balance-derived (WB) and calibrated (cal.) $S_{U,max}$ from all 16 study catchments. The symbols indicate the median $S_{U,max}$ for each method, the horizontal error bars indicate the range of feasible $S_{U,max}$ values (25th/75th percentiles) from the model, and vertical error bars indicate the min-max range obtained from several I_{max} values (colors as in Figure 1b).

L-band (SMAP-L-am_d, SMAP-L) products, while the lowest correlations are observed for AMSR2-C1-am with a median of $r = 0.63$ (Figure 8c). A higher sensitivity to soil moisture is expected for L-band retrievals over C and X band as a result of a higher penetration depth, a higher sensitivity of the dielectric constant to soil moisture, and an increased transmissivity of vegetation. SAR provides information at a higher spatial resolution compared to passive radiometers (Entekhabi et al., 2010). The reason explaining the lower correlations of AMSR2-C1-am is likely related to RFI. The AMSR2 low-resolution ascending products (overpass at 1.30 p.m.) show a higher degree of similarity with modeled root-zone water storage dynamics than the descending overpasses (Figure 8c). This is in line with findings from Brocca et al. (2011), despite the benefit of reduced difference between surface and canopy temperature of nighttime overpasses.

Similarly, lowest median correlations (r varying between 0.62 and 0.72) are found in the wettest, steep, and forested Ardennes catchments (IDs 1–5; Figure 8d) and highest (0.80–0.84) in the catchments with highest aridity index (IDs 13–16); see Table 1. Accuracies of soil moisture retrieval are indeed affected by a complex topography and high vegetation density (Brocca et al., 2017). It should be noted that the comparison of Spearman rank correlation is based on a different number of observations for each product (Table 2).

4.3. Influence of Catchment Characteristics on T_{opt}

Root-zone storage capacities $S_{U,max}$ were available as calibrated parameters from the hydrological model and from the water-balance approach described in sections 3.2 and S5. We calculate the 20-year return period root-zone water storage capacity for several values of the interception capacity I_{max}. Both approaches provide broadly consistent values with a Spearman rank correlation coefficient of $r = 0.67$ with $p = 0.004$ (and Pearson correlation of 0.86 with $p = 2e^{-5}$) for median values of $S_{U,max}$ retained as feasible and median $S_{U,max}$ values estimated from the water-balance approach (Figure 9).

High (median $r > 0.80$) and significant positive ($p < 0.05$) correlations are found between T_{opt} values of all soil moisture products and the calibrated root-zone water storage capacities $S_{U,max}$; see Table 3 and Figure 10a for a selection of products (all others shown in section S11). Spearman rank correlations between T_{opt} values and water-balance-derived root-zone storage capacities are less strong but still statistically significant ($p < 0.05$) for most soil moisture products (Table 3 and Figure 10b). The correlations are strongest for the S1-CSAR product ($r = 0.65$), while the weakest link was found with the AMSR2-C1-am product ($r = 0.36$). Similarly, T_{opt} in the AMSR2-C1-am product is less sensitive to $S_{U,max}$ ($dT_{opt}/dS_{U,max} = 0.23$ day mm^{-1}), possibly because of RFI, while the S1-CSAR product exhibits the highest sensitivity ($dT_{opt}/dS_{U,max} = 0.52$ day mm^{-1}), which is likely related to the larger spread in T_{opt} values (Figures 8a and 10b). In addition, all products suggest that T_{opt} is insensitive to $S_{U,max}$ at $S_{U,max}$ values below 100 mm, this could be related to the already very low T_{opt} (<6 days) in these catchments. The vertical error bars in Figure 10 suggest that T_{opt} is not very sensitive to the uncertainty in model parameters. While previous studies (Albergel et al., 2008; Paulik et al., 2014) showed an increase in T_{opt} for increasing depth of the soil profile, in line with equation (2), we explicitly make the link with root-zone storage capacity derived from runoff, precipitation, and evaporation data.

We found no significant correlations between T_{opt} and aridity index, runoff coefficient. or mean annual precipitation and potential evaporation (Table 3). Instead, the interplay between accumulated precipitation and actual evaporation during dry periods represented by the root-zone storage capacity $S_{U,max}$ shows a significant positive correlation with T_{opt}.

T_{opt} values are inversely correlated with the flashiness indices I_f of the study catchments (Table 3; Figure 10c), implying that a more flashy runoff (high flashiness index) indicates lower T_{opt} and, by extension, lower $S_{U,max}$ and therefore higher temporal variability in soil moisture.

Table 3
Spearman Rank Correlation Coefficients Between the Optimal Values of the Characteristic Time Length T_{opt} [d] per Product and the Calibrated (cal.) and Water-Balance-Derived (WB) Root-Zone Water Storage Capacities $S_{U,max}$, Mean Annual Precipitation (P), Potential Evaporation (E_p), Aridity Index (E_p/P), Runoff Ratio (Q/P), and Flashiness Index (I_f) and Percentage of Forest Cover (for.); Percentage of Agricultural Cover (agr.); Percentage of Highly Productive and Fissured Aquifers (fiss., Based on IHME); Percentage Clay, Sand, and Silt; Catchment Area; Drainage Density (dd); and Mean Slope

Product	$S_{U,max}$ (cal.)	$S_{U,max}$ (WB)	P	E_p	E_p/P	Q/P	I_f
S1-CSAR	0.87**	0.65*	−0.01	−0.32	−0.11	−0.16	−0.65**
SMAP-L-am_d	0.90**	0.56*	0.04	−0.43	−0.18	−0.17	−0.66*
SMAP-L	0.95**	0.60*	0.05	−0.39	−0.21	−0.05	−0.57*
AMSR2-X-am_d	0.80**	0.44	−0.34	−0.16	0.16	−0.44	−0.40
AMSR2-X-am	0.81**	0.56*	−0.24	−0.18	0.07	−0.38	−0.43
AMSR2-X-pm	0.92**	0.54*	−0.12	−0.40	−0.08	−0.22	−0.62*
AMSR2-C1-am_d	0.61*	0.37	−0.11	−0.39	−0.12	−0.14	−0.44
AMSR2-C1-am	0.57*	0.36	−0.20	−0.38	0.02	−0.33	−0.53*
AMSR2-C1-pm	0.85**	0.60*	0.02	−0.44	−0.19	−0.12	−0.60*
AMSR2-C2-am	0.90**	0.56*	0.01	−0.50*	−0.20	−0.11	−0.70*
AMSR2-C2-pm	0.82**	0.55*	−0.17	−0.28	−0.01	−0.31	−0.46

Product	for.	agr.	fiss.	clay	sand	silt	area	dd	slope
S1-CSAR	−0.45	0.83**	−0.01	−0.38	−0.29	0.77**	−0.42	0.07	−0.27
SMAP-L-am_d	−0.28	0.68*	−0.01	−0.49	−0.21	0.78**	−0.34	0.19	−0.21
SMAP-L	−0.30	0.67*	−0.13	−0.47	−0.15	0.69*	−0.28	0.11	−0.12
AMSR2-X-am_d	−0.45	0.80**	−0.02	−0.20	−0.26	0.59*	−0.44	0.09	−0.42
AMSR2-X-am	−0.41	0.82**	0.01	−0.24	−0.26	0.66*	−0.51*	−0.00	−0.44
AMSR2-X-pm	−0.30	0.78**	−0.09	−0.44	−0.17	0.68*	−0.39	0.22	−0.21
AMSR2-C1-am_d	−0.07	0.67*	−0.36	−0.33	0.03	0.51*	−0.37	0.33	−0.26
AMSR2-C1-am	−0.07	0.65*	−0.15	−0.48	−0.06	0.62*	−0.24	0.16	−0.25
AMSR2-C1-pm	−0.24	0.73*	−0.17	−0.51*	−0.25	0.83**	−0.37	0.16	−0.23
AMSR2-C2-am	−0.24	0.73*	−0.14	−0.54*	−0.20	0.78**	−0.32	0.18	−0.08
AMSR2-C2-pm	−0.31	0.74*	−0.05	−0.38	−0.19	0.66*	−0.40	0.12	−0.35

*$p < 0.05$. **$p < 0.001$.

We found significant positive correlations between T_{opt} and percentage agriculture (Table 3; Figure 10d), suggesting a low temporal variability of soil moisture in agriculture-dominated catchments, also implying higher $S_{U,max}$ values in these catchments, which are related to low runoff ratios and, therefore, high evaporation rates (Table 1). Interestingly, T_{opt} is positively related to percentage silt in a catchment (Table 3; Figure 10e) and therefore also to the percentage of agriculture, which is likely related to the fertility and suitability of silt for growing crops as it promotes water retention and air circulation. No significant relations are found between T_{opt} and the percentages of clay and sand (Tables 1 and 3 and section S11).

No significant relations between T_{opt} and geological features (percentage of highly productive aquifers) or topographic indicators (catchment area, drainage density, and mean slope) are found (see Table 3 and section S11).

5. Discussion

5.1. Advances

We found a median T_{opt} of 17 days, which is close to the often used value of 20 days (Wagner et al., 1999); however, we show that T_{opt} significantly varies between catchments (5th/95th percentiles of 1 and 98 days) and products (highest T_{opt} for S1-CSAR). This is in line with the variability reported by other studies. Ceballos et al. (2005) found values of approximately 50 days to represent the soil profile between 0 and 100 cm based on soil moisture measurements in agricultural fields in Spain. de Lange et al. (2008) mentions a general characteristic time length of 20 days based on observed and modeled soil moisture series, while Beck et al. (2009) found a T_{opt} value of 5 days for the calculation of SWI in Australian catchments.

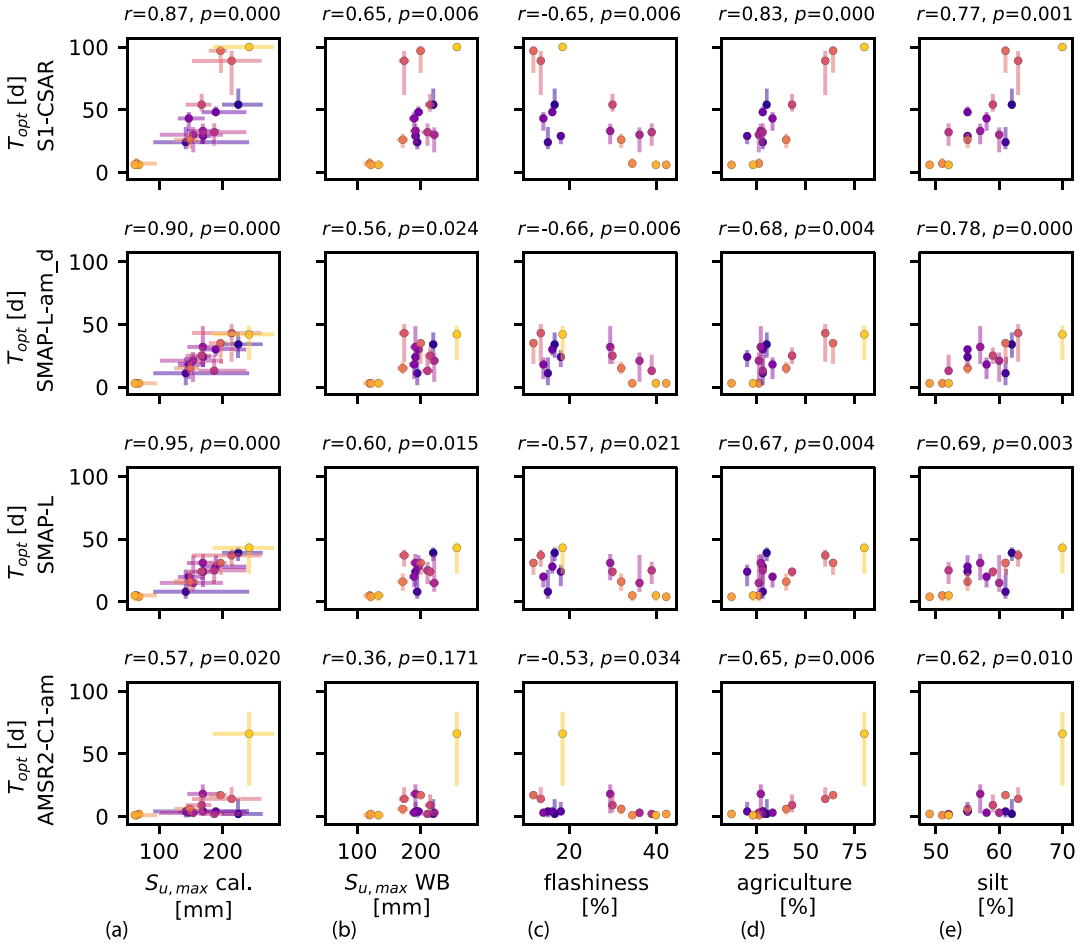

Figure 10. Optimal value of the characteristic time length T_{opt} (with vertical bars associated with the $25/75^{th}$ percentiles of T_{opt} from parameter sets kept as feasible) as a function of (a) calibrated root-zone water storage capacities ($S_{U,max}$ cal., median and $25/75^{th}$ percentiles of parameter sets kept as feasible), (b) water-balance-derived root-zone water storage capacities ($S_{U,max}$ WB, median and min-max range based on I_{max} values for a 20-year return period), (c) flashiness index, (d) percentage agriculture and (e) percentage silt for the 16 studied catchments for a selection of products (colors as in Figure 1b). Spearman rank coefficients r with associated p-values are calculated for the median values.

Previously, T_{opt} was shown to increase with increasing depth of the soil profile at the point scale (Albergel et al., 2008; Ceballos et al., 2005; Paulik et al., 2014; Wagner et al., 1999; Wang et al., 2017). However, T_{opt} was not linked to a defined storage in the subsurface at the catchment scale. Here, we explicitly show the increase of T_{opt} with increasing estimates of catchment-scale root-zone water storage capacities $S_{U,max}$. For modeling applications and data assimilation of satellite soil moisture products in runoff forecasting applications (Brocca et al., 2010; Laiolo et al., 2016; López López et al., 2017; Loizu et al., 2018; Wanders et al., 2014), our results suggest that suitable values of T can be inferred from a calibrated model or based on estimates of root-zone water storage capacities. These estimates can readily be determined using available hydrometeorological data, instead of selecting a standard value of 20 days based on the work of Wagner et al. (1999).

Albergel et al. (2008) and Wang et al. (2017) suggest that T values are low in areas with high evaporative demand and less frequent but more intense precipitation. The results from our water-balance approach rather suggest that these are typically areas where vegetation needs to overcome long dry spells and, therefore, with relatively large root-zone water storage capacities and T_{opt}. This is an important conclusion, as it shows that the interplay between precipitation and evaporation is the main climatic driver that controls T, and not the precipitation and evaporation individually, as often tested.

The highest T_{opt} values occur in agricultural-dominated catchments, which is in line with the relatively high values of T_{opt} (40–60 days) reported by Ceballos et al. (2005) in agricultural fields in Spain. In the Meuse, these catchments are characterized by low flashiness indices, low runoff ratios, and, therefore, high actual evaporation, resulting in a small temporal variability of soil moisture (high T_{opt}) and large root-zone water storage capacities $S_{U,max}$. The high agricultural cover also coincides with a relatively high silt percentage, related to the fertility and suitability of silt for growing crops due to the high water holding capacity. Soils with fine texture promote high water retention, slow drainage and, therefore, higher T_{opt} than soils with coarser textures, as also mentioned by Ceballos et al. (2005). These findings highlight the interactions between soil properties (% silt), the interplay between precipitation and evaporation ($S_{U,max}$), land cover (% agriculture), and runoff signatures (I_f) to characterize soil moisture behavior and estimate T_{opt} to infer root-zone from near-surface soil moisture.

SMAP-L-am_d, SMAP-L, and S1-CSAR derived times series of SWI show the highest similarity with modeled root-zone soil moisture S_U. The longer wavelength of L-band compared to C and X bands allows for a deeper soil penetration and a higher sensitivity to soil moisture. The difference in Spearman rank correlations between modeled root-zone soil moisture and SWI for the high- and low-resolution products is, therefore, less than between bands (Figure 8c). The advantage of S1-CSAR is the high spatial resolution to capture small-scale changes, easily missed out by coarse resolution sensors (Bauer-Marschallinger et al., 2019). During large scale and high intensity precipitation events from end of May until end of June 2016, the S1-CSAR product also shows the expected sharp increase in soil moisture, which is, for unknown reasons, missed by or relatively limited in most passive microwave products (Figure 7).

The variability of T_{opt} values is related to the soil moisture product itself. The larger variance of the near-surface soil moisture signal of S1-CSAR leads to a larger range of T_{opt} values (Figure 8a). Paulik et al. (2014) show a stronger agreement between in situ measurements and SWI compared to SSM, which could be related to noise being filtered out by the SWI. Our findings further suggest that T_{opt} values are likely to increase with increasing noise in the observations (section S9).

Both the remote sensing and the hydrological communities can benefit from our analysis, as it provides guidance for hydrologists to meaningfully infer root-zone soil moisture from near-surface soil moisture for hydrological applications, while it clarifies the behavior of T for several near-surface soil moisture products and its relation with hydrometeorological variables, soil texture, land cover, and runoff dynamics for the remote sensing community.

5.2. Limitations

In previous studies, T_{opt} was often estimated using observed soil moisture time series. However, these point observations often fail to represent the spatial heterogeneity at the catchment scale. In this study, we instead calibrate a process-based hydrological model (Figure 2a) against observed runoff to derive T_{opt} by relating the time series of SWI to modeled daily root-zone soil moisture S_U (Figures 6 and 7). However, it implies that the model provides a meaningful representation of true soil moisture at catchment scale. As we are interested in root-zone soil moisture and because T is a function of the depth of the layer below the surface (equation (2)), we related T_{opt} to root-zone water storage capacities $S_{U,max}$ estimated as a calibration parameter and, in an independent way, from a water-balance approach. The water-balance approach, however, also relies on assumptions related to estimation of the return period, interception evaporation, actual evaporation, groundwater losses, and periods where infiltration takes place and deficits start to accumulate. Yet the important additional information used in both methods is the runoff data, from which actual evaporation can be estimated and, by extension, the water storage capacity in the root zone, which influences root-zone soil moisture behavior.

As the selected catchments are relatively similar in size and all located in a temperate climate zone, an interesting next step would be to assess the relation between T_{opt} and $S_{U,max}$, land cover, and soil texture in a larger variety of catchments, differing in size and climate zone. We expect the positive correlation between T_{opt} and $S_{U,max}$ to be transferable to other areas, as the water-balance approach has successfully been applied in a variety of climate zones (New Zealand in de Boer-Euser et al., 2016; Australia in Donohue et al., 2012; and United States in Gentine et al., 2012, and Gao et al., 2014) or even globally (Wang-Erlandsson et al., 2016). The positive relation between agricultural cover, silt percentage, and T_{opt} found in the studied catchments might not apply in other areas, in contrast to the expected relation between T_{opt} and flashiness index.

Furthermore, the approach could be tested using several other models. However, if they provide a plausible long-term partitioning of water fluxes to evaporation and drainage from the root-zone soil moisture, we do not expect our results to be significantly affected by model selection. Additionally, our results with respect to differences in Spearman rank correlations between products could be affected if 10 years of satellite near-surface soil moisture data based on SMAP and Sentinel-1 would be available, instead of the less than 2 years of data available here.

6. Conclusion

The SWI enables us to infer root-zone soil moisture from satellite-based near-surface soil moisture, using an estimate of the characteristic time length (T) of the water flux from the surface to the root zone. Estimating T has so far proven difficult as no clear link with climate or soil has been established. Using a process-based lumped hydrological model calibrated on runoff data, we identified optimal T values (T_{opt}) that lead to the highest correlation between SWI and modeled root-zone soil moisture S_U in the Meuse basin (Figures 6 and 7). While the median T_{opt} value of 17 days approximates the often used standard value of 20 days, T_{opt} significantly varies between catchments and soil moisture products (5th/95th percentiles of 1 and 98 days; Figures 8a and 8b). In the past, T has been conceptually linked to an undefined storage volume in the subsurface. We now show for 16 contrasting catchments in the Meuse river basin that T is strongly and positively related with the root-zone water storage capacity (Figure 10). This catchment-scale vegetation accessible water storage capacity can be readily and robustly estimated based on water balance data. Our key finding implies that the interplay between precipitation and evaporation during dry periods, which regulates the size of the storage capacity in the unsaturated root zone, is the main driver controlling T_{opt} in temperate climates. Such a clear link between T_{opt} and hydrometeorological variables opens the opportunity to generate meaningful estimates of water contents in the root zone from globally available remotely sensed near-surface soil moisture data. These are of critical importance for hydrological and meteorological applications, as root-zone soil moisture controls how much water is available for plant transpiration and, therefore, the partitioning of precipitation to runoff and evaporation.

Acknowledgments
We thank Rijkswaterstaat and Deltares for the financial support to conduct this analysis. The authors would like to thank VanderSat for providing the soil moisture data and the Service Public de Wallonie, Direction générale opérationnelle de la Mobilité et des Voies hydrauliques, Département des Etudes et de l'Appui à la Gestion, and Direction de la Gestion hydrologique intégrée (Bld du Nord 8-5000 Namur, Belgium) for providing the precipitation and discharge data. The authors thank the editor Marc Bierkens and the three anonymous referees for their constructive comments, which helped us improve the manuscript. The data used in this study are described in the cited references and are available online in the 4TU data repository (https://doi.org/10.4121/uuid:c2d4ec46-a4d0-445c-99e9-58e0e3f86038; (Bouaziz, 2020)).

References

Albergel, C., de Rosnay, P., Balsamo, G., Isaksen, L., & Muñoz-Sabater, J. (2012). Soil moisture analyses at ECMWF: Evaluation using global ground-based in situ observations. *Journal of Hydrometeorology*, *13*(5), 1442–1460. https://doi.org/10.1175/jhm-d-11-0107.1

Albergel, C., Rüdiger, C., Pellarin, T., Calvet, J. C., Fritz, N., Froissard, F., et al. (2008). From near-surface to root-zone soil moisture using an exponential filter: An assessment of the method based on in-situ observations and model simulations. *Hydrology and Earth System Sciences*, *12*(6), 1323–1337. https://doi.org/10.5194/hess-12-1323-2008

Büttner, G., Soukup, T., & Kosztra, B. (2014). CLC2012 addendum to CLC2006 technical guidelines. Final Draft, Copenhagen (EEA).

Ballabio, C., Panagos, P., & Monatanarella, L. (2016). Mapping topsoil physical properties at European scale using the LUCAS database. *Geoderma*, *261*, 110–123. https://doi.org/10.1016/j.geoderma.2015.07.006

Banque Hydro (2018). Banque Hydro. Ministère de l'Ecologie, du Développement Durable et de l'Energie, available, last access 2018-07-13. Retrieved from https://hydro.eaufrance.fr/

Bauer-Marschallinger, B., Freeman, V., Cao, S., Paulik, C., Schaufler, S., Stachl, T., et al. (2019). Toward global soil moisture monitoring with Sentinel-1: Harnessing assets and overcoming obstacles. *IEEE Transactions on Geoscience and Remote Sensing*, *57*(1), 520–539. https://doi.org/10.1109/TGRS.2018.2858004

Beck, H. E., de Jeu, R. A. M., Bruijnzeel, L. A., Schellekens, J., & van Dijk, A. I. J. M. (2009). Improving curve number based storm runoff estimates using soil moisture proxies. *IEEE Journal of Selected Topics in Applied Earth Observations and Remote Sensing*, *2*(4), 250–259. https://doi.org/10.1109/JSTARS.2009.2031227

Blöschl, G., Bierkens, M. F. P., Chambel, A., Cudennec, C., Destouni, G., Fiori, A., et al. (2019). Twenty-three unsolved problems in hydrology (UPH) a community perspective. *Hydrological Sciences Journal*, *64*(10), 1141–1158. https://doi.org/10.1080/02626667.2019.1620507

Blöschl, G., & Zehe, E. (2005). On hydrological predictability. *Hydrological Processes*, *19*(19), 3923–3929. https://doi.org/10.1002/hyp.6075

Bogena, H. R., Herbst, M., Huisman, J. A., Rosenbaum, U., Weuthen, A., & Vereecken, H. (2010). Potential of wireless sensor networks for measuring soil water content variability. *Vadose Zone Journal*, *9*(4), 1002. https://doi.org/10.2136/vzj2009.0173

Bouaziz, L. J. E. (2020). Data underlying the research of: Improved understanding of the link between catchment-scale vegetation accessible storage and satellite-derived Soil Water Index. (Bouaziz et al. 2020, Water Resources Research). 4TU.Centre for Research Data. Dataset. doi: https://doi.org/10.4121/uuid:c2d4ec46-a4d0-445c-99e9-58e0e3f86038

Bouaziz, L., Weerts, A., Schellekens, J., Sprokkereef, E., Stam, J., Savenije, H., & Hrachowitz, M. (2018). Redressing the balance: Quantifying net intercatchment groundwater flows. *Hydrology and Earth System Sciences*, *22*(12), 6415–6434. https://doi.org/10.5194/hess-22-6415-2018

Brocca, L., Crow, W. T., Ciabatta, L., Massari, C., De Rosnay, P., Enenkel, M., et al. (2017). A review of the applications of ASCAT soil moisture products. *IEEE Journal of Selected Topics in Applied Earth Observations and Remote Sensing*, *10*(5), 2285–2306. https://doi.org/10.1109/JSTARS.2017.2651140

Brocca, L., Hasenauer, S., Lacava, T., Melone, F., Moramarco, T., Wagner, W., et al. (2011). Soil moisture estimation through ASCAT and AMSR-E sensors: An intercomparison and validation study across Europe. *Remote Sensing of Environment*, *115*(12), 3390–3408. https://doi.org/10.1016/j.rse.2011.08.003

Brocca, L., Melone, F., Moramarco, T., Wagner, W., & Hasenauer, S. (2010). ASCAT soil wetness index validation through in situ and modeled soil moisture data in central Italy. *Remote Sensing of Environment*, *114*(11), 2745–2755. https://doi.org/10.1016/j.rse.2010.06.009

Brocca, L., Melone, F., Moramarco, T., Wagner, W., Naeimi, V., Bartalis, Z., & Hasenauer, S. (2010). Improving runoff prediction through the assimilation of the ASCAT soil moisture product. *Hydrology and Earth System Sciences*, *14*(10), 1881–1893. https://doi.org/10.5194/hess-14-1881-2010

Budyko, M. I. (1961). The heat balance of the Earth's surface. *Soviet Geography*, *2*(4), 3–13.

Ceballos, A., Scipal, K., Wagner, W., & Martínez-Fernández, J. (2005). Validation of ERS scatterometer-derived soil moisture data in the central part of the Duero Basin, Spain. *Hydrological Processes*, *19*(8), 1549–1566. https://doi.org/10.1002/hyp.5585

Crow, W. T., Bindlish, R., & Jackson, T. J. (2005). The added value of spaceborne passive microwave soil moisture retrievals for forecasting rainfall-runoff partitioning. *Geophysical Research Letters*, *32*, L1840. https://doi.org/10.1029/2005GL023543

de Boer-Euser, T., McMillan, H. K., Hrachowitz, M., Winsemius, H. C., & Savenije, H. H. G. (2016). Influence of soil and climate on root zone storage capacity. *Water Resources Research*, *52*, 2009–2024. https://doi.org/10.1002/2015WR018115

de Lange, R., Beck, R., van de Giesen, N., Friesen, J., de Wit, A., & Wagner, W. (2008). Scatterometer-derived soil moisture calibrated for soil texture with a one-dimensional water-flow model. *IEEE Transactions on Geoscience and Remote Sensing*, *46*(12), 4041–4049. https://doi.org/10.1109/TGRS.2008.2000796

de Wit, M. J. M., Warmerdam, P. M. M., Torfs, P. J. J. F., Uijlenhoet, R., Roulin, E., Cheymol, A., et al. (2001). Effect of climate change on the hydrology of the river Meuse, Wageningen UR, the Netherlands, Technical Report. https://edepot.wur.nl/211994

Donohue, R. J., Roderick, M. L., & McVicar, T. R. (2012). Roots, storms and soil pores: Incorporating key ecohydrological processes into Budyko's hydrological model. *Journal of Hydrology*, *436-437*, 35–50. https://doi.org/10.1016/j.jhydrol.2012.02.033

Duan, Q., Sorooshian, S., & Gupta, V. K. (1994). Optimal use of the SCE-UA global optimization method for calibrating watershed models. *Journal of Hydrology*, *158*(3-4), 265–284. https://doi.org/10.1016/0022-1694(94)90057-4

Eagleson, P. S., & Tellers, T. E. (1982). Ecological optimality in water limited natural soil vegetation systems: 2. Tests and applications. *Water Resources Research*, *18*(2), 341–354. https://doi.org/10.1029/WR018i002p00341

Entekhabi, D., Das, N., Njoku, E. G., Johnson, T. J., & Shi, J. (2016). MAP L3 Radar/Radiometer Global Daily 9 km EASE-Grid Soil Moisture, Version 3. [L3 SM P E]. 10.5067/7KKNQ5UURM2W.

Entekhabi, D., Nakamura, H., & Njoku, E. G. (1994). Solving the inverse problem for soil moisture and temperature profiles by sequential assimilation of multifrequency remotely sensed observations. *IEEE Transactions on Geoscience and Remote Sensing*, *32*(2), 438–448. https://doi.org/10.1109/36.295058

Entekhabi, D., Njoku, E. G., O'Neill, P. E., Kellogg, K. H., Crow, W. T., Edelstein, W. N., et al. (2010). The Soil Moisture Active Passive (SMAP) Mission. *Proceedings of the IEEE*, *98*(5), 704–716. https://doi.org/10.1109/jproc.2010.2043918

Entekhabi, D., Yueh, S., O'Neill, P. E., Kellogg, K. H., Allen, A., Bindlish, R., et al. (2014). SMAP Handbook, Soil Moisture Active Passive. *National Aeronautics and Space Administration*. https://smap.jpl.nasa.gov/mission/description/

Euser, T., Hrachowitz, M., Winsemius, H. C., & Savenije, H. H. G. (2015). The effect of forcing and landscape distribution on performance and consistency of model structures. *Hydrological Processes*, *29*(17), 3727–3743. https://doi.org/10.1002/hyp.10445

Fenicia, F., Kavetski, D., Savenije, H. H. G., & Pfister, L. (2016). From spatially variable streamflow to distributed hydrological models: Analysis of key modeling decisions. *Water Resources Research*, *52*, 954–989. https://doi.org/10.1002/2015WR017398

Fenicia, F., McDonnell, J. J., & Savenije, H. H. G. (2008). Learning from model improvement: On the contribution of complementary data to process understanding. *Water Resources Research*, *44*, W06419. https://doi.org/10.1029/2007WR006386

Fenicia, F., Savenije, H. H. G., Matgen, P., & Pfister, L. (2006). Is the groundwater reservoir linear? Learning from data in hydrological modelling. *Hydrology and Earth System Sciences*, *10*(1), 139–150. https://doi.org/10.5194/hess-10-139-2006

Ford, T. W., Harris, E., & Quiring, S. M. (2014). Estimating root zone soil moisture using near-surface observations from SMOS. *Hydrology and Earth System Sciences*, *18*(1), 139–154. https://doi.org/10.5194/hess-18-139-2014

Fovet, O., Ruiz, L., Hrachowitz, M., Faucheux, M., & Gascuel-Odoux, C. (2015). Hydrological hysteresis and its value for assessing process consistency in catchment conceptual models. *Hydrology and Earth System Sciences*, *19*(1), 105–123. https://doi.org/10.5194/hess-19-105-2015

Gao, H., Hrachowitz, M., Schymanski, S. J., Fenicia, F., Sriwongsitanon, N., & Savenije, H. H. G. (2014). Climate controls how ecosystems size the root zone storage capacity at catchment scale. *Geophysical Research Letters*, *41*, 7916–7923. https://doi.org/10.1002/2014GL061668

Gentine, P., D'Odorico, P., Lintner, B. R., Sivandran, G., & Salvucci, G. (2012). Interdependence of climate, soil, and vegetation as constrained by the Budyko curve. *Geophysical Research Letters*, *39*, 2–7. https://doi.org/10.1029/2012GL053492

Gevaert, A. I., Renzullo, L. J., Van Dijk, A. I. J. M., Van Der Woerd, H. J., Weerts, A. H., & De Jeu, R. A. M. (2018). Joint assimilation of soil moisture retrieved from multiple passive microwave frequencies increases robustness of soil moisture state estimation. *Hydrology and Earth System Sciences*, *22*(9), 4605–4619. https://doi.org/10.5194/hess-22-4605-2018

Hooghart, J. C., & Lablans, W. N. (1988). *Van Penman naar Makkink: een nieuwe berekeningswijze voor de klimatologische verdampingsgetallen*. De Bilt, the Netherlands: De Bilt, Royal Netherlands Meteorological Institute (KNMI).

Hrachowitz, M., & Clark, M. P. (2017). HESS opinions: The complementary merits of competing modelling philosophies in hydrology. *Hydrology and Earth System Sciences*, *21*(8), 3953–3973. https://doi.org/10.5194/hess-21-3953-2017

Hrachowitz, M., Fovet, O., Ruiz, L., Euser, T., Gharari, S., Nijzink, R., et al. (2014). Process consistency in models: The importance of system signatures, expert knowledge, and process complexity. *Water Resources Research*, *50*, 7445–7469. https://doi.org/10.1002/2014WR015484

Hulsman, P., Winsemius, H. C., Michailovsky, C., Savenije, H. H. G., & Hrachowitz, M. (2019). Using altimetry observations combined with GRACE to select parameter sets of a hydrological model in data scarce regions. *Hydrology and Earth System Sciences Discussions*, *September*, 1–35. https://doi.org/10.5194/hess-2019-346

Kleidon, A., & Heimann, M. (1998). A method of determining rooting depth from a terrestrial biosphere model and its impacts on the global water and carbon cycle. *Global Change Biology*, *4*(3), 275–286. https://doi.org/10.1046/j.1365-2486.1998.00152.x

López López, P., Sutanudjaja, E. H., Schellekens, J., Sterk, G., & Bierkens, M. F. P. (2017). Calibration of a large-scale hydrological model using satellite-based soil moisture and evapotranspiration products. *Hydrology and Earth System Sciences*, *21*(6), 3125–3144. https://doi.org/10.5194/hess-21-3125-2017

López López, P., Wanders, N., Schellekens, J., Renzullo, L. J., Sutanudjaja, E. H., & Bierkens, M. F. P. (2016). Improved large-scale hydrological modelling through the assimilation of streamflow and downscaled satellite soil moisture observations. *Hydrology and Earth System Sciences*, *20*(7), 3059–3076. https://doi.org/10.5194/hess-20-3059-2016

Laiolo, P., Gabellani, S., Campo, L., Silvestro, F., Delogu, F., Rudari, R., et al. (2016). Impact of different satellite soil moisture products on the predictions of a continuous distributed hydrological model. *International Journal of Applied Earth Observation and Geoinformation*, *48*, 131–145. https://doi.org/10.1016/j.jag.2015.06.002

Leroux, D. J., Pellarin, T., Vischel, T., Cohard, J. M., Gascon, T., Gibon, F., et al. (2016). Assimilation of SMOS soil moisture into a distributed hydrological model and impacts on the water cycle variables over the Ouémé catchment in Benin. *Hydrology and Earth System Sciences*, *20*(7), 2827–2840. https://doi.org/10.5194/hess-20-2827-2016

Loizu, J., Massari, C., Álvarez-Mozos, J., Tarpanelli, A., Brocca, L., & Casalí, J. (2018). On the assimilation set-up of ASCAT soil moisture data for improving streamflow catchment simulation. *Advances in Water Resources*, *111*(November 2017), 86–104. https://doi.org/10.1016/j.advwatres.2017.10.034

Mahmood, R., & Hubbard, K. G. (2007). Relationship between soil moisture of near surface and multiple depths of the root zone under heterogeneous land uses and varying hydroclimatic conditions. *Hydrological Processes*, *21*(25), 3449–3462. https://doi.org/10.1002/hyp.6578

Manfreda, S., Brocca, L., Moramarco, T., Melone, F., & Sheffield, J. (2014). A physically based approach for the estimation of root-zone soil moisture from surface measurements. *Hydrology and Earth System Sciences*, *18*(3), 1199–1212. https://doi.org/10.5194/hess-18-1199-2014

McCabe, M. F., Rodell, M., Alsdorf, D. E., Miralles, D. G., Uijlenhoet, R., Wagner, W., et al. (2017). The future of Earth observation in hydrology. *Hydrology and Earth System Sciences*, *21*(7), 3879–3914. https://doi.org/10.5194/hess-21-3879-2017

Mezentsev, V. (1955). Back to the computation of total evaporation. *Meteorologia i Gidrologia*, *5*, 24–26.

Milly, P. C. D. (1994). Climate, interseasonal storage of soil water, and the annual water balance. *Advances in Water Resources*, *17*(1-2), 19–24. https://doi.org/10.1016/0309-1708(94)90020-5

Mostbauer, K., Kaitna, R., Prenner, D., & Hrachowitz, M. (2018). The temporally varying roles of rainfall, snowmelt and soil moisture for debris flow initiation in a snow-dominated system. *Hydrology and Earth System Sciences*, *22*(6), 3493–3513. https://doi.org/10.5194/hess-22-3493-2018

Nijzink, R. C., Almeida, S., Pechlivanidis, I. G., Capell, R., Gustafssons, D., Arheimer, B., et al. (2018). Constraining conceptual hydrological models with multiple information sources. *Water Resources Research*, *54*, 8332–8362. https://doi.org/10.1029/2017WR021895

Nijzink, R., Hutton, C., Pechlivanidis, I., Capell, R., Arheimer, B., Freer, J., et al. (2016). The evolution of root-zone moisture capacities after deforestation: A step towards hydrological predictions under change? *Hydrology and Earth System Sciences*, *20*(12), 4775–4799. https://doi.org/10.5194/hess-20-4775-2016

Nijzink, R. C., Samaniego, L., Mai, J., Kumar, R., Thober, S., Zink, M., et al. (2016). The importance of topography-controlled sub-grid process heterogeneity and semi-quantitative prior constraints in distributed hydrological models. *Hydrology and Earth System Sciences*, *20*(3), 1151–1176. https://doi.org/10.5194/hess-20-1151-2016

Owe, M., de Jeu, R., & Holmes, T. (2008). Multisensor historical climatology of satellite-derived global land surface moisture. *Journal of Geophysical Research*, *113*, F01002. https://doi.org/10.1029/2007JF000769

Parajka, J., Naeimi, V., Blöschl, G., & Komma, J. (2009). Matching ERS scatterometer based soil moisture patterns with simulations of a conceptual dual layer hydrologic model over Austria. *Hydrology and Earth System Sciences*, *13*(2), 259–271. https://doi.org/10.5194/hess-13-259-2009

Paulik, C., Dorigo, W., Wagner, W., & Kidd, R. (2014). Validation of the ASCAT Soil Water Index using in situ data from the International Soil moisture network. *International Journal of Applied Earth Observation and Geoinformation*, *30*(1), 1–8. https://doi.org/10.1016/j.jag.2014.01.007

Ragab, R. (1995). Towards a continuous operational system to estimate the root-zone soil moisture from intermittent remotely sensed surface moisture. *Journal of Hydrology*, *173*(1-4), 1–25. https://doi.org/10.1016/0022-1694(95)02749-F

Rakovec, O., Kumar, R., Mai, J., Cuntz, M., Thober, S., Zink, M., et al. (2016). Multiscale and multivariate evaluation of water fluxes and states over European river basins. *Journal of Hydrometeorology*, *17*(1), 287–307. https://doi.org/10.1175/JHM-D-15-0054.1

Sabater, J. M., Jarlan, L., Calvet, J.-C., Bouyssel, F., & De Rosnay, P. (2007). From near-surface to root-zone soil moisture using different assimilation techniques. *Journal of Hydrometeorology*, *8*(2), 194–206. https://doi.org/10.1175/jhm571.1

Savenije, H. H. G., & Hrachowitz, M. (2017). HESS Opinions "catchments as meta-organisms—A new blueprint for hydrological modelling". *Hydrology and Earth System Sciences*, *21*(2), 1107–1116. https://doi.org/10.5194/hess-21-1107-2017

Schenk, H. J., & Jackson, R. B. (2002). Rooting depths, lateral root spreads and below-ground/above-ground allometries of plants in water-limited ecosystems. *Journal of Ecology*, *90*(3), 480–494. https://doi.org/10.1046/j.1365-2745.2002.00682.x

Schymanski, S. J., Sivapalan, M., Roderick, M. L., Beringer, J., & Hutley, L. B. (2008). An optimality-based model of the coupled soil moisture and root dynamics. *Hydrology and Earth System Sciences*, *12*(3), 913–932. https://doi.org/10.5194/hess-12-913-2008

Service Public de Wallonie (2018). Service Public de Wallonie. Direction générale opérationnelle de la Mobilité et des Voies hydrauliques, Département des Etudes et de l'Appui à la Gestion, Direction de la Gestion hydrologique intégrée, Bld du Nord 8-5000 Namur, Belgium.

Sheffield, J., Wood, E. F., Pan, M., Beck, H., Coccia, G., Serrat-Capdevila, A., & Verbist, K. (2018). Satellite remote sensing for water resources management: Potential for supporting sustainable development in data-poor regions. *Water Resources Research*, *54*, 9724–9758. https://doi.org/10.1029/2017WR022437

Silvestro, F., Gabellani, S., Rudari, R., Delogu, F., Laiolo, P., & Boni, G. (2015). Uncertainty reduction and parameter estimation of a distributed hydrological model with ground and remote-sensing data. *Hydrology and Earth System Sciences*, *19*(4), 1727–1751. https://doi.org/10.5194/hess-19-1727-2015

Stroud, P. (1999). A recursive exponential filter for time-sensitive data. *Rep. LAUR-99*, 1–8. Retrieved from https://public.lanl.gov/stroud/ExpFilter/ExpFilter995573.pdf

Sutanudjaja, E. H., Van Beek, L. P. H., De Jong, S. M., Van Geer, F. C., & Bierkens, M. F. P. (2014). Calibrating a large-extent high-resolution coupled groundwater-land surface model using soil moisture and discharge data. *Water Resources Research*, *50*, 687–705. https://doi.org/10.1002/2013WR013807

Tian, S. (2007). Water resources research. *Journal of the American Water Resources Association*, *5*(3), 2–2. https://doi.org/10.1111/j.1752-1688.1969.tb04897.x

Trigo, I. F., Dacamara, C. C., Viterbo, P., Roujean, J. L., Olesen, F., Barroso, C., et al. (2011). The satellite application facility for land surface analysis. *International Journal of Remote Sensing*, *32*(10), 2725–2744. https://doi.org/10.1080/01431161003743199

Turc, L. (1954). Le Bilan d'eau des sols: Relations entre les précipitations, l'évaporation et l'écoulement. *Annales Agronomiques*, *5*, 491–595.

van Osnabrugge, B., Weerts, A. H., & Uijlenhoet, R. (2017). genRE: A method to extend gridded precipitation climatology data sets in near real-time for hydrological forecasting purposes. *Water Resources Research*, *53*, 9284–9303. https://doi.org/10.1002/2017WR021201

van der Schalie, R., Kerr, Y., Wignerond, J. P., Rodriguez-Fernandez, N. J., Al-Yaari, A., & de Jeu, R. A. M. (2016). Global SMOS soil moisture retrievals from the and parameter retrieval Model. *International Journal of Applied Earth Observation and Geoinformation*, *45*, 125–134. https://doi.org/10.1016/j.jag.2015.08.005

Wagner, W., Lemoine, G., & Rott, H. (1999). A method for estimating soil moisture from ERS Scatterometer and soil data. *Remote Sensing of Environment*, *70*(2), 191–207. https://doi.org/10.1016/S0034-4257(99)00036-X

Wanders, N., Karssenberg, D., De Roo, A., De Jong, S. M., & Bierkens, M. F. P. (2014). The suitability of remotely sensed soil moisture for improving operational flood forecasting. *Hydrology and Earth System Sciences*, *18*(6), 2343–2357. https://doi.org/10.5194/hess-18-2343-2014

Wang, T., Franz, T. E., You, J., Shulski, M. D., & Ray, C. (2017). Evaluating controls of soil properties and climatic conditions on the use of an exponential filter for converting near surface to root zone soil moisture contents. *Journal of Hydrology*, *548*, 683–696.

Wang-Erlandsson, L., Bastiaanssen, W. G. M., Gao, H., Jägermeyr, J., Senay, G. B., Van Dijk, A. I. J. M., et al. (2016). Global root zone storage capacity from satellite-based evaporation. *Hydrology and Earth System Sciences*, *20*(4), 1459–1481. https://doi.org/10.5194/hess-20-1459-2016